

NovoMolGen: Rethinking Molecular Language Model Pretraining

Kamran Chitsaz^{1,2,*}, Roshan Balaji^{5,6,7,*}, Quentin Fournier², Nirav Pravinbhai Bhatt^{5,6,7,8,†}, and Sarath Chandar^{1,2,3,4,†}

¹Chandar Research Lab, ²Mila – Quebec AI Institute, ³Polytechnique Montréal, ⁴Canada CIFAR AI Chair,

⁵BioSystems Engineering and Control Lab, ⁶Wadhwani School of Data Science and AI, IIT Madras, ⁷The Centre for Integrative Biology and Systems medicinE (IBSE), ⁸IIT Madras Zanzibar

* Equal Contribution, † Equal Supervision

Designing *de novo* molecules with desired property profiles requires efficient exploration of the vast chemical space ranging from 10^{23} to 10^{60} possible synthesizable candidates. While various deep generative models have been developed to design small molecules using diverse input representations, Molecular Large Language Models (Mol-LLMs) based on string representations have emerged as a scalable approach capable of exploring billions of molecules. However, there remains limited understanding regarding how standard language modeling practices such as textual representations, tokenization strategies, model size, and dataset scale impact molecular generation performance. In this work, we systematically investigate these critical aspects by introducing NovoMolGen, a family of transformer-based foundation models pretrained on 1.5 billion molecules for *de novo* molecule generation. Through extensive empirical analyses, we identify a weak correlation between performance metrics measured during pretraining and actual downstream performance, revealing important distinctions between molecular and general NLP training dynamics. NovoMolGen establishes new state-of-the-art results, substantially outperforming prior Mol-LLMs and specialized generative models in both unconstrained and goal-directed molecular generation tasks, thus providing a robust foundation for advancing efficient and effective molecular modeling strategies.

🤗 Model Weights: huggingface.co/chandar-lab/NovoMolGen

🔗 Code Repository: github.com/chandar-lab/NovoMolGen

1. Introduction

Discovering new drugs for oncology, immunology, and rare or infectious diseases remains challenging due to the cost and inefficiency of exhaustive experimental screening [Kirkpatrick and Ellis, 2004]. Efficient computational strategies are therefore essential to explore the vast chemical space and design synthesizable molecules with desired properties. Deep generative models have emerged as powerful tools for this task by learning complex structure–property relationships from large molecular datasets [Grisoni et al., 2020, Jin et al., 2020a, Podda et al., 2020, Mahmood et al., 2021, Hoogeboom et al., 2022]. A wide range of molecular representations has been explored, including vector-based [Rogers and Hahn, 2010], graph-based [Lee et al., 2023, Yang et al., 2024], 3D-based [Xu et al., 2023, Huang et al., 2023, Zhang et al., 2023], and string-based approaches. Among these, string-based formats such as SMILES [Weininger, 1988], DeepSMILES [O’Boyle and Dalke, 2018], SELFIES [Krenn et al., 2022], and SAFE [Noutahi et al., 2024] are particularly scalable. Their text-based structure is memory-efficient and compatible with modern language models, making them well-suited for large-scale pretraining on datasets like GDB-13 [Ruddigkeit et al., 2012] and ZINC [Tingle et al., 2023], which contain billions of molecules.

Building on this foundation, Molecular Language Models (Mol-LLMs) have shown strong promise for automated molecule generation. Early models such as REINVENT [Olivecrona et al., 2017] used RNNs with reinforcement learning to generate goal-directed molecules. Later works like MolGPT [Bagal et al., 2022], SMILES-GPT [Adilov, 2021], and BindGPT [Zholus et al., 2024] adopted autoregressive transformers, leveraging BPE tokenization and capturing both syntax and semantics of SMILES. Encoder-decoder models such as BARTSmiles [Chilingaryan et al., 2022] and MolGen [Fang et al., 2023] further improved robustness and validity through denoising and self-feedback mechanisms.

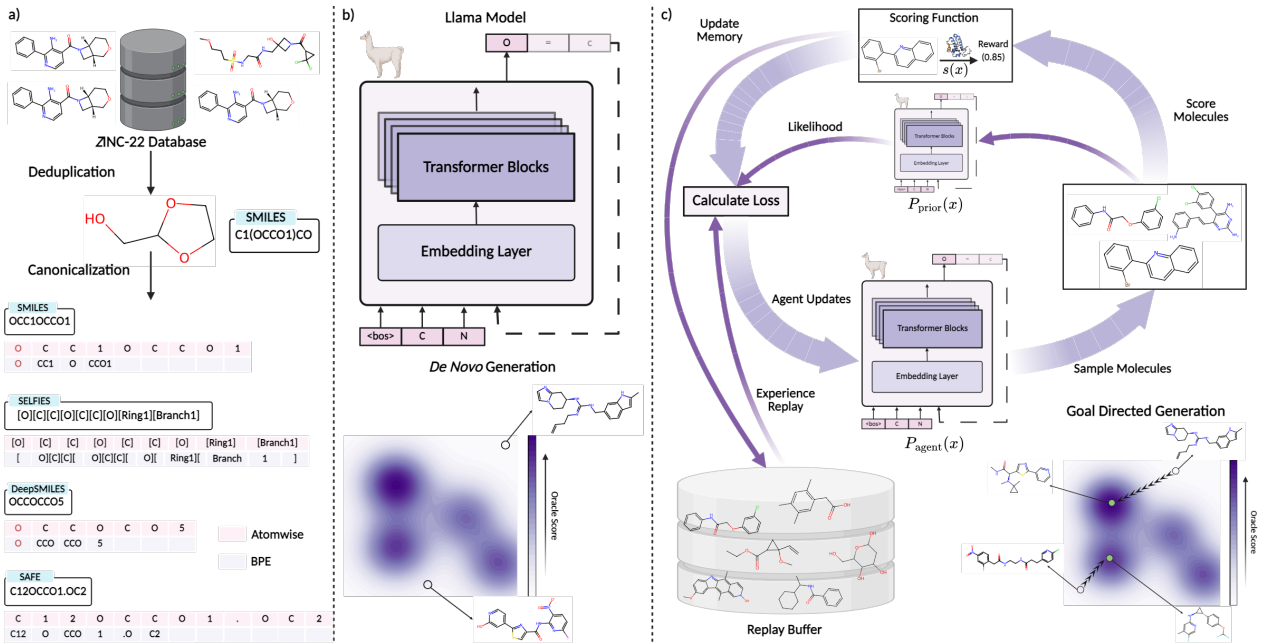


Figure 1: Four-stages of NovoMolGen pipeline: (a) SMILES deduplication, canonicalization, and conversion to SELFIES, SAFE, and DeepSMILES, with Atomwise and Byte Pair Encoding (BPE) tokenization. (b) Pretraining of NovoMolGen and unconstrained molecular generation along the learned manifold. (c) Reinforcement learning-based fine-tuning for goal-directed molecular design.

Scaling the pretraining of molecular language models has demonstrated strong potential for improving molecular generation and representation learning. SAFE-GPT [Noutahi et al., 2024] exemplifies this trend, training an 87M-parameter GPT-like architecture on 1.1B SAFE strings to improve fragment-based design, enabling scaffold decoration, motif extension, and linker generation. *f*-RAG [Lee et al., 2024a] leverages the SAFE-GPT architecture in combination with a fragment injection module, which suggests additional fragments based on input fragments to complete and generate novel molecules. Building on SMILES-based pretraining, MoLFormer [Ross et al., 2022] employs linear attention and rotary embeddings to pretrain a transformer encoder on 1.1 billion SMILES. GP-MoLFormer [Ross et al., 2024] extends this approach to autoregressive generation, training a 46.8M-parameter decoder on 1.1 billion SMILES and investigating the trade-off between novelty and memorization at extreme scales.

While molecular language models draw inspiration from recent breakthroughs in natural language processing (NLP), directly applying LLM methodologies to molecular generation presents unique challenges. Small molecule representations impose fundamentally different constraints compared to natural languages, with shorter sequence lengths, smaller vocabularies, and highly structured syntax that affects how models capture chemical relationships. Despite progress in the development of individual string-based models, a fundamental question remains: *“How can we best tailor and optimize language modeling techniques for the unique chemical specificities of small molecules?”* This paper addresses the question through a large-scale, systematic investigation of the key factors influencing model performance. Frey et al. [2023] examines neural scaling behavior in large chemical models by varying model and dataset sizes; however, their analysis is limited to pretraining loss and does not extend to downstream molecular optimization tasks, which are more indicative of practical performance. Yu et al. [2024] explores molecular generation in the context of a broader chemistry-focused AI assistant, but relies primarily on basic metrics such as validity and fingerprint Tanimoto similarity. Similarly, Özçelik and Grisoni [2024] employs a considerably smaller dataset (~1.5M molecules) and focuses on evaluation metrics such as Fréchet ChemNet Distance (FCD), which, while informative, offer a narrower assessment of generation quality. While the work of Skinnider et al. [2021] provides valuable strategies for low-data environments, its applicability to large-scale pretraining is limited. Moreover, the study’s conclusions are derived from experiments using RNN architectures, limiting the direct comparability of its findings to those from modern, transformer-based foundation models.

To date, no systematic study has examined how architectural decisions and training protocols influence the validity, diversity, and property optimizability of generated molecules. Furthermore, while pretraining improves molecular representations, its impact on downstream task performance remains poorly understood. This highlights the need to investigate how the different aspects of the Mol-LLMs pipeline affect both pretraining efficiency and fine-tuning effectiveness, ensuring that Mol-LLMs generalize well to real-world molecular design challenges. To bridge these gaps in the existing work and to address open questions in Mol-LLM design, we make the following key contributions in this work:

- We introduce **NovoMolGen**, a family of transformer-based models pretrained on 1.5 billion molecules, and present the largest systematic study (>30,000 experiments) to date on Mol-LLMs by evaluating the effects of molecular representation, tokenization, model scaling, and dataset size on *de novo* generation.
- We investigate the impact of model scaling, observing that while increasing model size shows some trends in goal-directed generation tasks, it does not lead to consistent improvements across all metrics.
- We analyze SMILES, SELFIES, SAFE, and DeepSMILES with both atomwise and BPE tokenization and observe only modest performance differences overall. SMILES with BPE tokenization delivers the most consistent (albeit marginal) gains across FCD, Practical Molecular Optimization (PMO) and docking benchmarks, making it a practical default.
- We find that pretraining saturates early, and common proxy metrics like FCD correlate poorly with downstream PMO performance. Notably, even the earliest checkpoints outperform strong baselines, suggesting that essential chemical syntax is learned early.

To facilitate reproducibility we open-source our models, datasets, and code, establishing a comprehensive benchmark for advancing large-scale pretraining in Mol-LLMs.

2. Methodology

This section outlines our four-stage Mol-LLM pipeline (Figure 1). First, we preprocess 1.5B molecules from ZINC-22 using various representations (§2.1). Next, we pretrain transformer models on these representations (§2.2). Finally, fine-tuning with reinforcement learning optimizes task-specific reward functions (§2.3).

2.1. Data Preparation

We use the ZINC-22 database, the largest publicly available molecular library (\approx 70B synthesizable compounds as of Sept 2024), as the source for pretraining. Molecules are encoded in SMILES and organized based on their heavy atom count, which ranges from 4 to 49. To ensure diversity, we randomly sample 1.5B molecules using a stratified strategy based on heavy atom count, followed by deduplication and SMILES canonicalization. To our knowledge, this is the largest dataset used for *de novo* molecule generation pretraining. To study representation effects, we convert SMILES to SELFIES, SAFE, and DeepSMILES. To promote structural diversity, we enforce an average Tanimoto similarity below 0.5 within each batch. Details are provided in Appendix B.

For evaluation, we construct two validation sets. First, a 10M molecules scaffold-based split using Bemis–Murcko scaffolds [Bemis and Murcko, 1996], ensuring no scaffold overlap with the training set, in line with established protocols [Wu et al., 2018, Polykovskiy et al., 2020], to test the model’s generalization. While more precise alternatives (e.g., Butina, UMAP) exist [Guo et al., 2024], they are computationally infeasible at our scale. Second, we sample 10M molecules randomly from the remaining data to form a random validation set, capturing chemically diverse but training-aligned examples. Together, these sets offer complementary views on generalization and overfitting.

2.2. Pretraining

We employ autoregressive decoder-only transformers, a natural and effective architecture for *de novo* molecule generation. Trained via next-token prediction on string-based representations, these models inherently learn the principles of chemical syntax and validity in a left-to-right manner. This approach enables the generation of diverse and plausible molecules while efficiently capturing both local and global dependencies within large-scale chemical datasets.

While encoder-based architectures are powerful for learning rich, bidirectional molecular representations for predictive tasks (e.g., property prediction), their non-autoregressive nature makes them fundamentally less suited for the sequential, generative process required for *de novo* molecule design. Thus, the decoder-only paradigm remains the more direct and appropriate choice for our generative objectives. We adopt the Llama architecture [Dubey et al., 2024] and explore two tokenization strategies. Atomwise tokenization [Schwaller et al., 2019] segments molecules into chemically meaningful units (atoms, bonds, stereochemistry), while BPE [Kudo, 2018], trained on 100M molecules with a vocab size of 500 and dropout 0.1, captures frequent substructures and balances granularity and efficiency.

We pretrain three model sizes (32M, 157M, 300M parameters) to study scaling effects. Architecture choices follow the width-to-depth ratio proposed by Levine et al. [2020]. Training is done with FlashAttention [Dao et al., 2024] integrated into HuggingFace’s Trainer [Wolf et al., 2019], allowing large batch sizes and significantly improving training speed. Each model is trained with fixed global batch size of 19,200 (1.2M tokens/step) across 4×A100 GPUs. We use the AdamW optimizer with a cosine learning rate schedule peaking at 6×10^{-4} . Further training details appear in Appendix C and training curves are provided in Appendix D.

2.3. Fine-Tuning

Fine-tuning is essential in *de novo* molecule generation to align pretrained models with task-specific objectives (e.g., drug-likeness, bioactivity), especially under oracle budget constraints that demand high sample efficiency. We adopt and extend the REINVENT framework [Olivecrona et al., 2017], a well-established reinforcement learning (RL) approach shown to perform competitively against more complex policy optimizers like PPO [Bou et al., 2024, Schulman et al., 2017], while offering robustness and ease of implementation.

The method uses a fixed pretrained prior model, $P_{\text{prior}}(x)$, and a trainable agent, $P_{\text{agent}}(x)$, which is optimized to generate molecules x that maximize a task-specific reward function, $s(x)$. To enhance exploration and focus the optimization on high-quality candidates, we adapt the learning objective by incorporating a top- k sampling strategy, a concept central to the Augmented Hill-Climb method [Thomas et al., 2022]. In our implementation, the loss is computed exclusively on the subset of the top- k highest-scoring molecules generated in each batch, without applying diversity filters.

The agent is trained to minimize the cost function $J(X_k)$ over this subset of top- k molecules, X_k , defined as:

$$J(X_k) = \frac{1}{k} \sum_{x \in X_k} [\log P_{\text{prior}}(x) - \log P_{\text{agent}}(x) + \sigma \cdot s(x)]^2 \quad (1)$$

where σ is a scaling factor that controls the influence of the reward function $s(x)$. This loss function creates a learning objective that balances the generation of high-reward molecules with adherence to the chemically valid distribution of the prior model. Additionally, we use a penalty term,

$$J_p(X_k) = \frac{-1}{\frac{1}{k} \sum_{x \in X_k} \log P_{\text{agent}}(x)},$$

to discourage the generation of molecules with extremely low likelihoods under the agent’s learned distribution. This regularization prevents degenerate solutions, promotes confidence in the agent’s predictions, and enhances training stability. The final objective combines these components:

$$J_\theta = J + \lambda \cdot J_p, \quad (2)$$

where λ is a hyperparameter that weights the penalty term. To enhance sample efficiency and stabilize training, we incorporate an experience replay buffer [Guo and Schwaller, 2024]. The buffer stores the 100 top-performing molecules generated during fine-tuning, which are used to reinforce high-reward candidates and is pre-initialized with task specific top-100 molecules from the ZINC250k dataset [Irwin et al., 2012]. Further implementation details are available in Appendix E.

3. Experiments

We evaluate our models using distribution learning metrics (§3.1), analyzing the effects of model size (§3.2), molecular representation (§3.3), and tokenization (§3.4). Downstream performance is tested on the PMO

Table 1: Comprehensive performance metrics for baseline models and **NovoMolGen** (Random validation set). The baselines for CharRNN, VAE, and JT-VAE are sourced from Polykovskiy et al. [2020], while the results for LIMO, MolGen-7B, and GP-Molformer are taken from Ross et al. [2024]. **Blue** denotes the best performing model, while **Pink** represents the second-best performing model (p value < 0.05).

REPRESENTATION	TOKENIZATION	MODEL SIZE	Valid (\uparrow)	IntDiv (\uparrow)	Novelty (\uparrow)	FCD (\downarrow)	SNN (\uparrow)	Frag (\uparrow)	Scaff (\uparrow)
<i>Train</i>	–	–	1.000	1.000	0.0	0.0376	0.4657	0.9999	0.5144
CHARRNN [Polykovskiy et al., 2020]	Atomwise	–	0.9748	0.856	–	0.0732	0.6015	0.9998	0.9242
VAE [Polykovskiy et al., 2020]	Atomwise	–	0.9767	0.855	–	0.0990	0.6257	0.9994	0.9386
JT-VAE [Jin et al., 2018]	Atomwise	–	1.000	0.855	–	0.3954	0.5477	0.9965	0.8964
LIMO [Eckmann et al., 2022]	Atomwise	–	1.000	0.854	–	26.78	0.2464	0.6989	0.0079
MOLGEN-7B [Fang et al., 2023]	Atomwise	7B	1.000	0.855	–	0.0435	0.5138	0.9999	0.6538
GP-MOLFORMER [Ross et al., 2024]	Atomwise	46.8M	1.000	0.865	0.390	0.0591	0.5045	0.9998	0.7383
NOVOMOLGEN-SMILES	Atomwise	32M	0.999	0.851	0.983	0.0394	0.4657	0.9999	0.5309
		157M	0.999	0.851	0.981	0.0426	0.4656	0.9999	0.5200
		300M	0.999	0.851	0.981	0.0419	0.4657	0.9999	0.5219
	BPE	32M	0.999	0.851	0.982	0.0384	0.4654	0.9999	0.5182
		157M	0.999	0.852	0.980	0.0384	0.4655	0.9999	0.5193
		300M	0.999	0.851	0.979	0.0380	0.4657	0.9999	0.5173
NOVOMOLGEN-SELFIES	Atomwise	32M	1.000	0.852	0.982	0.0799	0.4651	0.9996	0.4765
	BPE	32M	1.000	0.851	0.984	0.0386	0.4649	0.9999	0.5105
NOVOMOLGEN-DEEPSMILES	Atomwise	32M	0.999	0.851	0.981	0.0400	0.4661	0.9999	0.5218
	BPE	32M	0.997	0.851	0.982	0.0380	0.4655	0.9999	0.5165
NOVOMOLGEN-SAFE	Atomwise	32M	0.957	0.853	0.953	0.9475	0.4562	0.9955	0.4521
	BPE	32M	0.997	0.852	0.976	0.3283	0.4599	0.9972	0.4913

benchmark (§3.5) and molecular docking tasks (§3.6). We also track training dynamics and metric progression (§3.7). Training and validation losses are tracked on both random and scaffold-based splits. All results use the 75000 step checkpoint (one full epoch). This checkpoint was selected because, as shown in Figure 3, key performance metrics had already saturated, with negligible improvements observed from further training.

3.1. Generation and Evaluation

We evaluated the pretrained models by sampling 30,000 molecules using temperature sampling ($T = 1.0$) without top- k or top- p filtering, as shown in Table 1. Generated molecules were assessed using standard metrics, including Validity, Novelty, Internal Diversity (IntDiv), Fréchet ChemNet Distance (FCD), Similarity to Nearest Neighbor (SNN), and fragment and scaffold similarities based on BRICS and Bemis–Murcko decompositions. Metrics that require a reference distribution (e.g., FCD, SNN) were computed using a 175,000-molecule subset from the random validation set. Notably, we exclude Novelty for most baselines since prior work typically computes it with respect to the much smaller MOSES dataset (≈ 1.5 M molecules), whereas our models were trained on the larger ZINC-22 set (1.5B molecules), making such comparisons inconsistent. Similar limitations affect other distribution-based metrics such as SNN and Scaffold Similarity. To enable fair evaluation, we also report results relative to the training-validation overlap (*Train*). Full definitions for our evaluation metrics are provided in Appendix F. Additional results, including scaffold-based splits and property distributions, can be found in Appendix G and Appendix H, respectively.

3.2. Impact of Model Size

We evaluated models with 32M, 157M, and 300M parameters using atomwise tokenization and compared them to the GP-MolFormer baseline, which follows a similar training pipeline but employs linear attention. In contrast, our models use full self-attention and are part of a broader study covering tokenization, molecular representation, and scaling. Across most metrics, including Validity, Fragment, and FCD, our models perform comparably, while significantly outperforming GP-MolFormer in Novelty, highlighting stronger exploration of chemical space. Increasing model size from 32M to 300M offers limited gains. Key metrics like SNN, FCD, and Fragment Similarity remain stable, indicating that even smaller models effectively capture core chemical patterns. Given their lower computational cost, smaller models such as the 32M variant present a practical and competitive option for molecular generation.

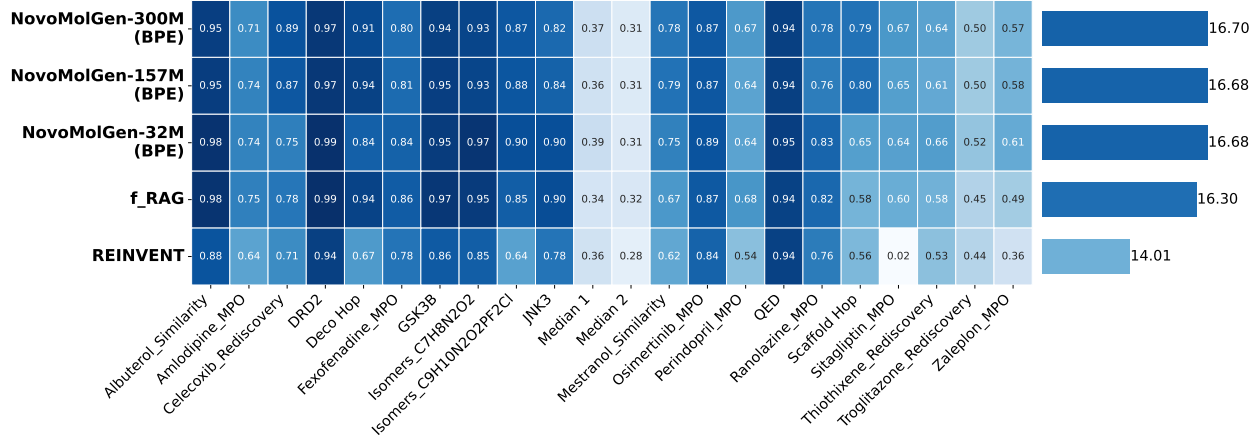


Figure 2: PMO benchmark results for NovoMolGen-SMILES across different model sizes: The heatmap (left) displays scores (average AUC top-10) for each task, while the bar chart (right) shows total scores, where higher values indicate better performance. **NovoMolGen-SMILES-300M (BPE)** achieves the highest overall score, outperforming other model variants. Results for REINVENT and *f*-RAG are taken directly from their respective publications.

3.3. Impact of Molecular Representation

To evaluate the impact of molecular representation, we pre-trained 32M models using SMILES, SELFIES, SAFE, and DeepSMILES with atomwise and BPE tokenization. As shown in Table 1, our analysis reveals that no single representation is universally optimal, with each presenting distinct trade-offs. For instance, while SELFIES guarantees 100% molecular validity, it tends to produce molecules with lower structural diversity (Scaffold Similarity and SNN). Conversely, SAFE struggles with distributional alignment, as indicated by a poor FCD score. When comparing our models to GP-MoLFormer, it is crucial to consider the differences in their pre-training data, which is a likely confounding factor. Our models were trained solely on ZINC, which emphasizes drug-like and synthesizable compounds. In contrast, GP-MoLFormer was trained on PubChem, a broader and more diverse chemical space that includes a wider variety of exotic moieties, natural products, and compounds with annotated bioactivity data that are largely absent in ZINC. This difference likely explains GP-MoLFormer’s higher internal diversity scores, despite its lower Novelty in our experiments. Considering the observed trade-offs, SMILES emerges as a robust and well-balanced representation, delivering strong and reliable performance across the majority of key metrics without the specific drawbacks of the alternatives.

3.4. Impact of Tokenization

We compare atomwise and BPE tokenization across molecular representations (Table 1) and observe that both schemes perform comparably across most metrics, including Validity, IntDiv, SNN, Frag, and Scaffold similarity. The only consistent differences appear in FCD, where BPE achieves slightly lower (better) scores, and in a modest increase in Novelty for SELFIES and DeepSMILES. While the observed differences in FCD are minor, BPE’s inherent efficiency makes it a compelling choice for molecular generation. BPE constructs a compact vocabulary where tokens often represent meaningful chemical substructures (shown in Figure K30), resulting in shorter sequence lengths and faster computation. This efficiency, combined with its consistent performance advantage, positions BPE as a pragmatic default choice for molecular generation tasks.

3.5. Goal-Directed Molecular Optimization: PMO Benchmark

We assess the goal-directed generation capabilities of NovoMolGen using the Practical Molecular Optimization (PMO) benchmark [Gao et al., 2022]. To ensure a rigorous and fair comparison, we strictly adhere to the evaluation settings proposed by Gao et al. [2022], which include a variety of drug discovery-relevant tasks and a constrained budget of 10,000 oracle function evaluations for each task.

Table 2: Performance of NovoMolGen (SMILES) on protein-ligand docking. The results are the means and standard deviations of 3 independent runs. For each target, we report the **novel top 5% docking score (DS) (kcal/mol)** and the **novel hit ratio (HR) (%)**. Higher hit ratios (\uparrow) and lower docking scores (\downarrow) indicate better performance. **Blue** denotes the best performing model, while **Pink** represents the second-best performing model (p value < 0.05).

Method	parp1		fa7		5ht1b		braf		jak2	
	DS (\downarrow)	HR (%) (\uparrow)	DS (\downarrow)	HR (%) (\uparrow)	DS (\downarrow)	HR (%) (\uparrow)	DS (\downarrow)	HR (%) (\uparrow)	DS (\downarrow)	HR (%) (\uparrow)
REINVENT	-8.70(0.52)	0.48(0.34)	-7.21(0.26)	0.21(0.08)	-8.77(0.32)	2.45(0.56)	-8.39(0.40)	0.13(0.09)	-8.17(0.28)	0.61(0.17)
MORLD	-7.53(0.26)	0.05(0.05)	-6.26(0.17)	0.01(0.01)	-7.87(0.65)	0.88(0.74)	-8.04(0.34)	0.05(0.04)	-7.82(0.13)	0.23(0.12)
HierVAE	-9.49(0.28)	0.55(0.21)	-6.81(0.27)	0.01(0.01)	-8.08(0.25)	0.51(0.28)	-8.98(0.53)	0.21(0.22)	-8.29(0.37)	0.23(0.13)
FREED-QS	-10.58(0.10)	4.63(0.73)	-8.38(0.04)	1.33(0.11)	-10.71(0.18)	16.77(0.90)	-10.56(0.08)	2.94(0.36)	-9.74(0.02)	5.80(0.30)
GDSS	-9.97(0.03)	1.93(0.21)	-7.78(0.04)	0.37(0.10)	-9.46(0.10)	4.67(0.31)	-9.22(0.07)	0.17(0.13)	-8.93(0.09)	1.17(0.28)
MOOD	-10.87(0.11)	7.02(0.43)	-8.16(0.07)	0.73(0.14)	-11.15(0.04)	18.67(0.42)	-11.06(0.03)	5.24(0.29)	-10.15(0.06)	9.20(0.52)
GEAM	-12.89(0.16)	40.56(0.82)	-9.89(0.12)	20.71(1.87)	-12.37(0.04)	38.48(0.35)	-12.34(0.10)	27.90(1.82)	-11.82(0.07)	42.95(1.11)
<i>f</i> -RAG	-12.95(0.05)	-	-9.90(0.21)	-	-12.67(0.14)	-	-12.39(0.05)	-	-11.84(0.32)	-
32M-ATOMWISE	-13.92(0.19)	77.13(9.40)	-11.11(0.36)	74.67(5.44)	-12.15(0.09)	53.98(4.87)	-12.43(0.21)	50.36(7.54)	-12.33(0.67)	79.31(8.82)
157M-ATOMWISE	-14.20(0.61)	84.58(2.31)	-10.77(0.25)	65.85(9.72)	-12.97(0.72)	63.57(5.45)	-12.73(0.16)	69.97(6.85)	-12.27(0.29)	77.38(8.95)
300M-ATOMWISE	-14.27(0.60)	77.73(8.39)	-11.20(0.26)	82.57(2.93)	-13.54(0.57)	67.83(2.47)	-13.10(0.50)	71.64(7.83)	-11.97(0.12)	81.23(1.30)
32M-BPE	-14.90(0.36)	90.24(1.36)	-11.70(0.46)	82.55(1.13)	-12.80(0.17)	64.92(5.51)	-13.80(0.20)	68.03(3.05)	-12.47(0.21)	79.24(6.43)
157M-BPE	-14.61(0.30)	84.41(3.65)	-11.53(0.06)	83.20(3.02)	-13.45(0.23)	64.71(3.09)	-13.13(0.71)	69.28(9.32)	-12.93(0.60)	77.35(9.94)
300M-BPE	-14.80(0.10)	81.46(5.78)	-11.67(0.49)	83.65(7.27)	-13.60(0.17)	69.33(4.26)	-13.40(0.30)	74.87(6.73)	-13.07(0.16)	84.89(3.10)

For each PMO task, we fine-tuned our pretrained models using the reinforcement learning-based fine-tuning approach described in Section 2.3. To ensure a fair comparison, we first performed an exhaustive hyperparameter search using the Perindopril_MPO and Zaleplon_MPO tasks, optimizing hyperparameters across three different random seeds per setting. The best hyperparameter configurations were then applied to fine-tune all PMO tasks. We evaluate different models with 32M, 157M, and 300M parameters using both atomwise and BPE tokenization to assess their impact on optimization performance. We benchmark our method against four key baselines: **REINVENT** [Olivecrona et al., 2017], a top performer in the original PMO analysis [Gao et al., 2022]; ***f*-RAG** [Lee et al., 2024a], the current state-of-the-art; and two genetic algorithms, **Graph-GA** [Gao et al., 2022] and **Mol-GA** [Tripp and Hernández-Lobato, 2023].

In Figure 2, we present the results for NovoMolGen across different model sizes for BPE tokenization with SMILES representation. NovoMolGen consistently outperforms both baselines, achieving substantial improvements over REINVENT and surpassing *f*-RAG across most tasks. Moreover, we observe that the smallest 32M model already demonstrates strong sample efficiency and achieves higher rewards on both Multi-Property Optimization (Perindopril, Zaleplon) and Bioactivity Optimization (JNK3, GSK3 β) tasks. Increasing the model size beyond this yields diminishing and often negligible gains. This aligns with our findings in Section 3.2, where all model sizes performed similarly in the distribution learning benchmark based on the pretraining data. Detailed results, including means, standard deviations, top molecule visualizations, reward curve and additional metrics, are provided in Appendix I.

3.6. Goal-Directed Molecular Optimization: Protein-Ligand Docking

To validate our *de novo* molecular generation model, we evaluated its performance in designing novel molecules with high binding affinity, favorable drug-like properties, and high synthesizability. Our approach is compared against established methods across five diverse protein targets: *parp1*, *fa7*, *5ht1b*, *braf*, and *jak2*, following the experimental framework of Lee et al. [2023]. For each target, we generated 3,000 molecules and quantified performance using two primary metrics. For both metrics, only unique molecules with a Tanimoto similarity below 0.4 to the training set are considered. The first metric, **Novel Hit Ratio (%)**, measures the percentage of novel molecules classified as “hits.” A molecule is defined as a hit if it satisfies three criteria: its docking score is lower than the median of known active molecules, QED > 0.5 , and SA < 5 . The second metric, **Novel Top 5% Docking Score**, then evaluates the quality of the top-generated candidates by computing the average docking score of the top 5% of novel molecules that also meet the drug-likeness filters of QED ≥ 0.5 and SA ≤ 5 .

We compare our models against several state-of-the-art baselines. These include fragment-based methods that assemble molecular substructures, such as **Hier-VAE** [Jin et al., 2020b], **FREED** [Yang et al., 2021], **GEAM** [Lee et al., 2024b], and ***f*-RAG**. We also benchmark against reinforcement learning agents operating on different

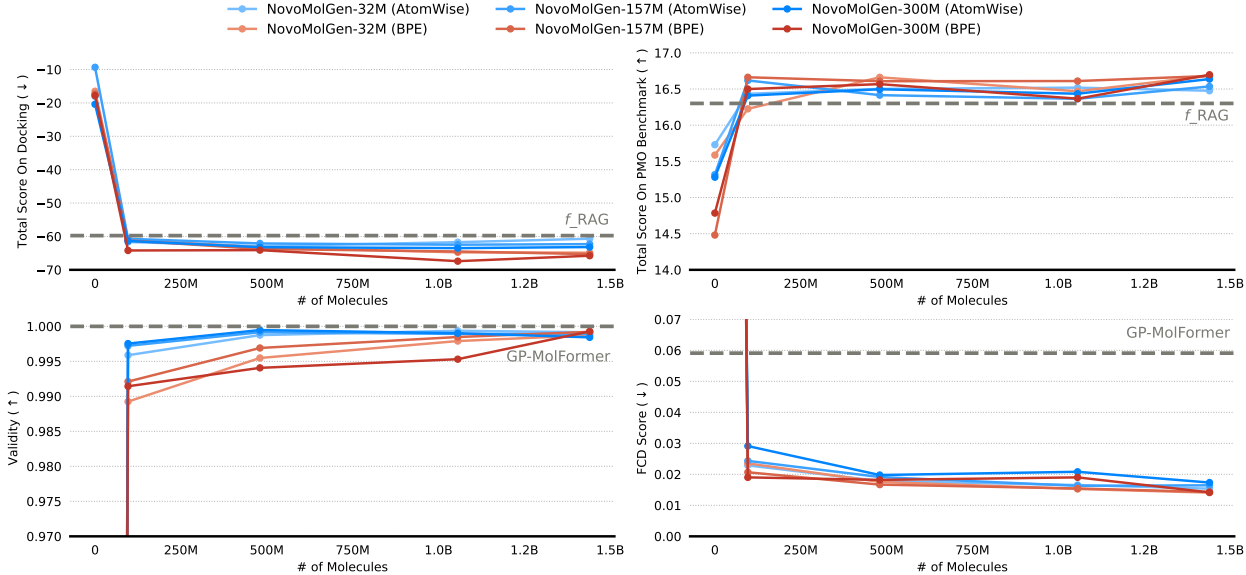


Figure 3: Performance saturation during pretraining: We plot key metrics for models of varying sizes (32M–300M) at intermediate checkpoints against the number of molecules seen. The results consistently show that performance saturates early, with diminishing returns for extended training.

representations: **REINVENT** on SMILES strings and **MORLD** [Jeon and Kim, 2020] on molecular graphs. Lastly, we include **MOOD** [Lee et al., 2023], a diffusion model that uses out-of-distribution control to enhance novelty.

In Table 2, we report the performance of NovoMolGen (SMILES) models with BPE and atomwise tokenization across different model sizes. Our models consistently outperform all baselines on both docking score (DS) and hit ratio (HR) metrics. Notably, scaling from 32M to 300M parameters yields only modest and inconsistent gains, reinforcing the observation from Section 3.2 that model architecture and training strategy are more critical than scale. Moreover, our models achieve significantly higher hit ratios that are often more than double those of strong baselines like GEAM. Additional details on protein targets, docking score computation, molecule visualizations, extended baselines, reward curve and supplementary metrics are provided in Appendix J.

3.7. Progression of Metrics During Pretraining

A central question in the training of Mol-LLMs is whether performance saturates over time and how this progression correlates with generative quality. To investigate this, we tracked multiple metrics throughout the pretraining process for models of varying sizes (32M, 157M, and 300M) using different tokenization strategies for the SMILES molecular representation. The progression of the total PMO score, Fréchet ChemNet Distance (FCD), and total docking score as a function of the number of molecules seen during pretraining is presented in Figure 3.

Our analysis reveals that the performance on downstream tasks saturates remarkably early, with extended pretraining and increased model scale yielding diminishing returns. To quantify the value of pretraining foundation models, we compared our models against identical architectures initialized with random weights and found that even a brief pretraining phase provides a substantial and immediate performance jump. As shown in our experiments, the earliest pretraining checkpoint already surpasses strong baselines like *f*-RAG on goal-directed generation tasks. While distributional metrics such as FCD show a more gradual and sustained improvement over time, the rapid plateau suggests that foundational chemical syntax (as shown by validity) is acquired very early in training. Subsequent training appears to primarily refine this understanding rather than unlocking significant new capabilities for these tasks.

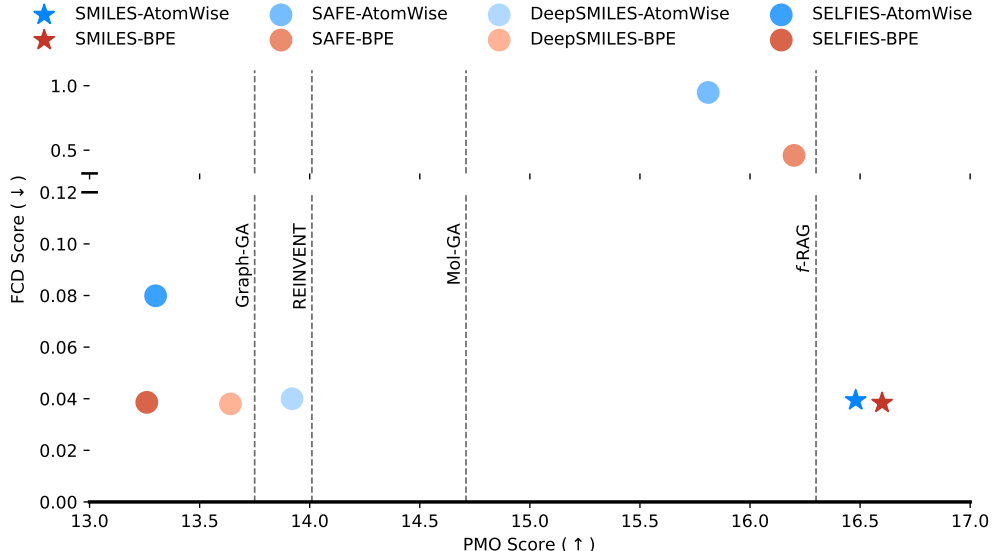


Figure 4: FCD does not correlate with downstream task performance: The plot compares the FCD score (y-axis, lower is better) against the aggregated PMO benchmark score (x-axis, higher is better) for models trained on various molecular representations and tokenization schemes.

4. Discussion

Our large-scale empirical analysis, encompassing over 30,000 experiments and the evaluation of more than one billion molecules, reveals a critical divergence in the training dynamics of Mol-LLMs compared to their natural language counterparts. While NLP models typically benefit from extensive training, performance on key molecular generation metrics, including PMO and docking scores, saturates early during pretraining. This is underscored by the unique observation that even the earliest checkpoint of our smallest model (32M parameters) surpasses strong baselines like REINVENT and *f*-RAG after fine-tuning. The early saturation suggests that extended self-supervised pretraining on large-scale chemical libraries offers diminishing returns for many molecular design tasks. Furthermore, our findings highlight a critical disconnect between standard pretraining metrics and actual downstream performance. As shown in Figure 4, models that achieve the best FCD scores (e.g., DeepSMILES (BPE)) often exhibit only modest downstream performance, whereas top-performing models on the PMO benchmark (e.g., SAFE) have sub-optimal FCD scores. The low correlation ($r = 0.376, p = 0.358$) challenges the utility of distribution-based metrics like FCD as reliable predictors of a model’s functional capabilities in goal-directed generation.

We posit that this rapid performance saturation is not an inherent limitation of the transformer architecture but rather a consequence of the fundamental constraints of current pre-training datasets and objectives. Unlike genomic or proteomic data, where evolutionary pressure has embedded a rich and functional learning signal, the large-scale chemical libraries commonly used for pre-training offer a comparatively weak signal. Libraries such as ZINC are curated primarily for synthetic accessibility, meaning their dominant signal teaches models chemical syntax rather than functional semantics. While datasets of natural products could provide a more biologically relevant signal, their limited scale curtails their utility for pre-training large models. Consequently, models pre-trained on existing chemical libraries quickly master the syntactic patterns of molecular strings but fail to learn the deeper, function-oriented principles essential for effective goal-directed design.

Based on these findings, we argue that future progress in molecular generation requires a paradigm shift away from objectives focused solely on chemical validity. Models should be guided by contextual signals early in training in combination with self-supervision. This can be achieved by incorporating objectives related to protein-ligand interactions, physicochemical properties, or experimental bioactivity. Furthermore, introducing reinforcement learning at earlier stages can provide a “fitness” signal analogous to natural selection, aligning generation with functional goals. By enriching the training process with such signals, future models can be

guided to master not only chemical syntax but also the functional utility crucial for solving real-world challenges in drug discovery.

5. Conclusion

We conducted a broad exploration of how different model sizes, molecular representations, tokenization strategies, and training protocols affect the capabilities of Mol-LLMs. NovoMolGen, which we pretrained on 1.5B molecules in multiple string-based formats, establishes state-of-the-art performance in both unconstrained generation and goal-directed optimization, surpassing the existing Mol-LLMs and specialized generative approaches. Notably, our findings challenge NLP-inspired assumptions about the necessity of extensive training or larger models, suggesting that performance can saturate relatively early. These observations provide a practical framework for building scalable, task-focused molecular foundation models and underscore the need for more demanding benchmarks that capture the true complexity of medicinal chemistry. Beyond its benchmark performance, NovoMolGen’s architecture provides a robust foundation for diverse future applications, from complex predictive tasks like retrosynthesis to text-instructed design [Fallahpour et al., 2025] and fragment-constrained generation [Thomas et al., 2024]. These avenues highlight the potential for well-designed models to serve as cornerstones for the next generation of multi-modal, goal-oriented molecular design tools.

6. Acknowledgement

Sarath Chandar is supported by the Canada CIFAR AI Chairs program, the Canada Research Chair in Lifelong Machine Learning, and the NSERC Discovery Grant. Roshan Balaji acknowledges support from the Prime Minister’s Research Fellowship (PMRF), India, and Nirav Bhatt acknowledges support from the Ministry of Education, Government of India. Both Roshan Balaji and Nirav Bhatt are also supported by the Wadhwani School of Data Science and AI, IIT Madras. The authors gratefully acknowledge the computational resources provided by Mila, Compute Canada, IBSE, and the Wadhwani School of Data Science and AI.

References

Sanjar Adilov. Generative Pre-Training from Molecules, September 2021. URL <https://chemrxiv.org/engage/chemrxiv/article-details/6142f60742198e8c31782e9e>.

Amr Alhossary, Stephanus Daniel Handoko, Yuguang Mu, and Chee-Keong Kwoh. Fast, accurate, and reliable molecular docking with QuickVina 2. *Bioinformatics*, 31(13):2214–2216, July 2015. ISSN 1367-4803. doi: 10.1093/bioinformatics/btv082. URL <https://doi.org/10.1093/bioinformatics/btv082>.

Viraj Bagal, Rishal Aggarwal, P. K. Vinod, and U. Deva Priyakumar. MolGPT: Molecular Generation Using a Transformer-Decoder Model. *Journal of Chemical Information and Modeling*, 62(9):2064–2076, May 2022. ISSN 1549-9596. doi: 10.1021/acs.jcim.1c00600. URL <https://doi.org/10.1021/acs.jcim.1c00600>. Publisher: American Chemical Society.

Guy W. Bemis and Mark A. Murcko. The Properties of Known Drugs. 1. Molecular Frameworks. *Journal of Medicinal Chemistry*, 39(15):2887–2893, January 1996. ISSN 0022-2623. doi: 10.1021/jm9602928. URL <https://doi.org/10.1021/jm9602928>. Publisher: American Chemical Society.

Albert Bou, Morgan Thomas, Sebastian Dittert, Carles Navarro, Maciej Majewski, Ye Wang, Shivam Patel, Gary Tresadern, Mazen Ahmad, Vincent Moens, et al. Acegen: Reinforcement learning of generative chemical agents for drug discovery. *Journal of Chemical Information and Modeling*, 64(15):5900–5911, 2024.

Marc Brockschmidt. GNN-FiLM: Graph Neural Networks with Feature-wise Linear Modulation. In *Proceedings of the 37th International Conference on Machine Learning*, pages 1144–1152. PMLR, November 2020. URL <https://proceedings.mlr.press/v119/brockschmidt20a.html>. ISSN: 2640-3498.

Nicola De Cao and Thomas Kipf. MolGAN: An implicit generative model for small molecular graphs, September 2022. URL <http://arxiv.org/abs/1805.11973>. arXiv:1805.11973 [stat].

Gayane Chilingaryan, Hovhannes Tamoyan, Ani Tevosyan, Nelly Babayan, Lusine Khondkaryan, Karen Ham-bardzumyan, Zaven Navoyan, Hrant Khachatrian, and Armen Aghajanyan. BARTSmiles: Generative Masked Language Models for Molecular Representations, November 2022. URL <http://arxiv.org/abs/2211.16349>. arXiv:2211.16349 [cs, q-bio].

Tri Dao, Daniel Y. Fu, Stefano Ermon, Atri Rudra, and Christopher Ré. FLASHATTENTION: fast and memory-efficient exact attention with IO-awareness. In *Proceedings of the 36th International Conference on Neural Information Processing Systems*, NIPS '22, pages 16344–16359, Red Hook, NY, USA, April 2024. Curran Associates Inc. ISBN 978-1-7138-7108-8.

Jörg Degen, Christof Wegscheid-Gerlach, Andrea Zaliani, and Matthias Rarey. On the Art of Compiling and Using 'Drug-Like' Chemical Fragment Spaces. *ChemMedChem*, 3(10):1503–1507, 2008. ISSN 1860-7187. doi: 10.1002/cmdc.200800178. URL <https://onlinelibrary.wiley.com/doi/abs/10.1002/cmdc.200800178>. _eprint: <https://onlinelibrary.wiley.com/doi/pdf/10.1002/cmdc.200800178>.

Abhimanyu Dubey, Abhinav Jauhri, Abhinav Pandey, Abhishek Kadian, Ahmad Al-Dahle, Aiesha Letman, Akhil Mathur, Alan Schelten, Amy Yang, Angela Fan, et al. The llama 3 herd of models. *arXiv preprint arXiv:2407.21783*, 2024.

Joseph L. Durant, Burton A. Leland, Douglas R. Henry, and James G. Nourse. Reoptimization of MDL Keys for Use in Drug Discovery. *Journal of Chemical Information and Computer Sciences*, 42(6):1273–1280, November 2002. ISSN 0095-2338. doi: 10.1021/ci010132r. URL <https://doi.org/10.1021/ci010132r>. Publisher: American Chemical Society.

Peter Eckmann, Kunyang Sun, Bo Zhao, Mudong Feng, Michael Gilson, and Rose Yu. LIMO: Latent Inceptionism for Targeted Molecule Generation. In *Proceedings of the 39th International Conference on Machine Learning*, pages 5777–5792. PMLR, June 2022. URL <https://proceedings.mlr.press/v162/eckmann22a.html>. ISSN: 2640-3498.

Adibvafa Fallahpour, Andrew Magnuson, Purav Gupta, Shihao Ma, Jack Naimer, Arnav Shah, Haonan Duan, Omar Ibrahim, Hani Goodarzi, Chris J Maddison, et al. Bioreason: Incentivizing multimodal biological reasoning within a dna-llm model. *arXiv preprint arXiv:2505.23579*, 2025.

Xiaomin Fang, Lihang Liu, Jieqiong Lei, Donglong He, Shanzhuo Zhang, Jingbo Zhou, Fan Wang, Hua Wu, and Haifeng Wang. Geometry-enhanced molecular representation learning for property prediction. *Nature Machine Intelligence*, 4(2):127–134, February 2022. ISSN 2522-5839. doi: 10.1038/s42256-021-00438-4. URL <https://www.nature.com/articles/s42256-021-00438-4>. Publisher: Nature Publishing Group.

Yin Fang, Ningyu Zhang, Zhuo Chen, Lingbing Guo, Xiaohui Fan, and Huajun Chen. Domain-Agnostic Molecular Generation with Chemical Feedback. In *The Twelfth International Conference on Learning Representations*, October 2023. URL <https://openreview.net/forum?id=9rPyHyjfwP>.

Nathan C Frey, Ryan Soklaski, Simon Axelrod, Siddharth Samsi, Rafael Gomez-Bombarelli, Connor W Coley, and Vijay Gadepally. Neural scaling of deep chemical models. *Nature Machine Intelligence*, 5(11):1297–1305, 2023.

Wenhai Gao, Tianfan Fu, Jimeng Sun, and Connor W. Coley. Sample Efficiency Matters: A Benchmark for Practical Molecular Optimization, October 2022. URL <http://arxiv.org/abs/2206.12411>. arXiv:2206.12411.

Niklas W. A. Gebauer, Michael Gastegger, and Kristof T. Schütt. Symmetry-adapted generation of 3d point sets for the targeted discovery of molecules. In *Proceedings of the 33rd International Conference on Neural Information Processing Systems*, pages 7566–7578. Curran Associates Inc., Red Hook, NY, USA, December 2019.

Justin Gilmer, Samuel S. Schoenholz, Patrick F. Riley, Oriol Vinyals, and George E. Dahl. Neural message passing for Quantum chemistry. In *Proceedings of the 34th International Conference on Machine Learning - Volume 70*, ICML'17, pages 1263–1272, Sydney, NSW, Australia, August 2017. JMLR.org.

Francesca Grisoni, Michael Moret, Robin Lingwood, and Gisbert Schneider. Bidirectional Molecule Generation with Recurrent Neural Networks. *Journal of Chemical Information and Modeling*, 60(3):1175–1183, March 2020. ISSN 1549-9596. doi: 10.1021/acs.jcim.9b00943. URL <https://doi.org/10.1021/acs.jcim.9b00943>. Publisher: American Chemical Society.

Dirk Groeneveld, Iz Beltagy, Pete Walsh, Akshita Bhagia, Rodney Kinney, Oyvind Tafjord, Ananya Harsh Jha, Hamish Ivison, Ian Magnusson, Yizhong Wang, Shane Arora, David Atkinson, Russell Author, Khyathi Raghavi Chandu, Arman Cohan, Jennifer Dumas, Yanai Elazar, Yuling Gu, Jack Hessel, Tushar Khot, William Merrill, Jacob Morrison, Niklas Muennighoff, Aakanksha Naik, Crystal Nam, Matthew E. Peters, Valentina Pyatkin, Abhilasha Ravichander, Dustin Schwenk, Saurabh Shah, Will Smith, Emma Strubell, Nishant Subramani, Mitchell Wortsman, Pradeep Dasigi, Nathan Lambert, Kyle Richardson, Luke Zettlemoyer, Jesse Dodge, Kyle Lo, Luca Soldaini, Noah A. Smith, and Hannaneh Hajishirzi. OLMo: Accelerating the Science of Language Models, June 2024. URL <http://arxiv.org/abs/2402.00838>. arXiv:2402.00838 [cs].

Jeff Guo and Philippe Schwaller. Saturn: Sample-efficient generative molecular design using memory manipulation. *arXiv preprint arXiv:2405.17066*, 2024.

Qianrong Guo, Saiveth Hernandez-Hernandez, and Pedro J Ballester. Scaffold splits overestimate virtual screening performance. In *International Conference on Artificial Neural Networks*, pages 58–72. Springer, 2024.

Zhichun Guo, Kehan Guo, Bozhao Nan, Yijun Tian, Roshni G. Iyer, Yihong Ma, Olaf Wiest, Xiangliang Zhang, Wei Wang, Chuxu Zhang, and Nitesh V. Chawla. Graph-based Molecular Representation Learning. In *Proceedings of the Thirty-Second International Joint Conference on Artificial Intelligence, IJCAI-23*, volume 6, pages 6638–6646, August 2023. doi: 10.24963/ijcai.2023/744. URL <https://www.ijcai.org/proceedings/2023/744>. ISSN: 1045-0823.

Rafael Gómez-Bombarelli, Jennifer N. Wei, David Duvenaud, José Miguel Hernández-Lobato, Benjamín Sánchez-Lengeling, Dennis Sheberla, Jorge Aguilera-Iparraguirre, Timothy D. Hirzel, Ryan P. Adams, and Alán Aspuru-Guzik. Automatic Chemical Design Using a Data-Driven Continuous Representation of Molecules. *ACS Central Science*, 4(2):268–276, February 2018. ISSN 2374-7943. doi: 10.1021/acscentsci.7b00572. URL <https://doi.org/10.1021/acscentsci.7b00572>. Publisher: American Chemical Society.

Jonathan Ho, Ajay Jain, and Pieter Abbeel. Denoising diffusion probabilistic models. In *Proceedings of the 34th International Conference on Neural Information Processing Systems*, NIPS '20, pages 6840–6851, Red Hook, NY, USA, December 2020. Curran Associates Inc. ISBN 978-1-7138-2954-6.

Emiel Hoogeboom, Víctor Garcia Satorras, Clément Vignac, and Max Welling. Equivariant Diffusion for Molecule Generation in 3D. In *Proceedings of the 39th International Conference on Machine Learning*, pages 8867–8887. PMLR, June 2022. URL <https://proceedings.mlr.press/v162/hoogeboom22a.html>. ISSN: 2640-3498.

Lei Huang, Hengtong Zhang, Tingyang Xu, and Ka-Chun Wong. MDM: Molecular Diffusion Model for 3D Molecule Generation. *Proceedings of the AAAI Conference on Artificial Intelligence*, 37(4):5105–5112, June 2023. ISSN 2374-3468. doi: 10.1609/aaai.v37i4.25639. URL <https://ojs.aaai.org/index.php/AAAI/article/view/25639>. Number: 4.

John J Irwin, Teague Sterling, Michael M Mysinger, Erin S Bolstad, and Ryan G Coleman. Zinc: a free tool to discover chemistry for biology. *Journal of chemical information and modeling*, 52(7):1757–1768, 2012.

Ross Irwin, Spyridon Dimitriadis, Jiazen He, and Esben Jannik Bjerrum. Chemformer: a pre-trained transformer for computational chemistry. *Machine Learning: Science and Technology*, 3(1):015022, January 2022. ISSN 2632-2153. doi: 10.1088/2632-2153/ac3ffb. URL <https://dx.doi.org/10.1088/2632-2153/ac3ffb>. Publisher: IOP Publishing.

Woosung Jeon and Dongsup Kim. Autonomous molecule generation using reinforcement learning and docking to develop potential novel inhibitors. *Scientific reports*, 10(1):22104, 2020.

Albert Q. Jiang, Alexandre Sablayrolles, Arthur Mensch, Chris Bamford, Devendra Singh Chaplot, Diego de las Casas, Florian Bressand, Gianna Lengyel, Guillaume Lample, Lucile Saulnier, Lélio Renard Lavaud, Marie-Anne Lachaux, Pierre Stock, Teven Le Scao, Thibaut Lavril, Thomas Wang, Timothée Lacroix, and William El Sayed. Mistral 7B, October 2023. URL <http://arxiv.org/abs/2310.06825>. arXiv:2310.06825 [cs].

Wengong Jin, Regina Barzilay, and Tommi Jaakkola. Junction Tree Variational Autoencoder for Molecular Graph Generation. In *Proceedings of the 35th International Conference on Machine Learning*, pages 2323–2332. PMLR, July 2018. URL <https://proceedings.mlr.press/v80/jin18a.html>. ISSN: 2640-3498.

Wengong Jin, Dr Regina Barzilay, and Tommi Jaakkola. Multi-Objective Molecule Generation using Interpretable Substructures. In *Proceedings of the 37th International Conference on Machine Learning*, pages 4849–4859. PMLR, November 2020a. URL <https://proceedings.mlr.press/v119/jin20b.html>. ISSN: 2640-3498.

Wengong Jin, Regina Barzilay, and Tommi Jaakkola. Hierarchical generation of molecular graphs using structural motifs. In *Proceedings of the 37th International Conference on Machine Learning*, volume 119 of *ICML’20*, pages 4839–4848. JMLR.org, July 2020b.

Jaehyeong Jo, Seul Lee, and Sung Ju Hwang. Score-based Generative Modeling of Graphs via the System of Stochastic Differential Equations. In *Proceedings of the 39th International Conference on Machine Learning*, pages 10362–10383. PMLR, June 2022. URL <https://proceedings.mlr.press/v162/jo22a.html>. ISSN: 2640-3498.

Thomas N. Kipf and Max Welling. Semi-Supervised Classification with Graph Convolutional Networks. In *International Conference on Learning Representations*, February 2017. URL <https://openreview.net/forum?id=SJU4ayYgl>.

Peter Kirkpatrick and Clare Ellis. Chemical space. *Nature*, 432(7019):823–823, December 2004. ISSN 1476-4687. doi: 10.1038/432823a. URL <https://www.nature.com/articles/432823a>. Publisher: Nature Publishing Group.

Lingkai Kong, Jiaming Cui, Haotian Sun, Yuchen Zhuang, B. Aditya Prakash, and Chao Zhang. Autoregressive Diffusion Model for Graph Generation. In *Proceedings of the 40th International Conference on Machine Learning*, pages 17391–17408. PMLR, July 2023. URL <https://proceedings.mlr.press/v202/kong23b.html>. ISSN: 2640-3498.

Mario Krenn, Qianxiang Ai, Senja Barthel, Nessa Carson, Angelo Frei, Nathan C. Frey, Pascal Friederich, Théophile Gaudin, Alberto Alexander Gayle, Kevin Maik Jablonka, Rafael F. Lameiro, Dominik Lemm, Alston Lo, Seyed Mohamad Moosavi, José Manuel Nápoles-Duarte, AkshatKumar Nigam, Robert Pollice, Kohulan Rajan, Ulrich Schatzschneider, Philippe Schwaller, Marta Skreta, Berend Smit, Felix Strieth-Kalthoff, Chong Sun, Gary Tom, Guido Falk von Rudorff, Andrew Wang, Andrew D. White, Adamo Young, Rose Yu, and Alán Aspuru-Guzik. SELFIES and the future of molecular string representations. *Patterns*, 3(10):100588, October 2022. ISSN 2666-3899. doi: 10.1016/j.patter.2022.100588. URL <https://www.sciencedirect.com/science/article/pii/S2666389922002069>.

Taku Kudo. Subword Regularization: Improving Neural Network Translation Models with Multiple Subword Candidates. In Iryna Gurevych and Yusuke Miyao, editors, *Proceedings of the 56th Annual Meeting of the Association for Computational Linguistics (Volume 1: Long Papers)*, pages 66–75, Melbourne, Australia, July 2018. Association for Computational Linguistics. doi: 10.18653/v1/P18-1007. URL <https://aclanthology.org/P18-1007/>.

Maksim Kuznetsov and Daniil Polykovskiy. MolGrow: A Graph Normalizing Flow for Hierarchical Molecular Generation. *Proceedings of the AAAI Conference on Artificial Intelligence*, 35(9):8226–8234, May 2021. ISSN 2374-3468. doi: 10.1609/aaai.v35i9.17001. URL <https://ojs.aaai.org/index.php/AAAI/article/view/17001>. Number: 9.

Tuan Le, Robin Winter, Frank Noé, and Djork-Arné Clevert. Neuraldecipher – reverse-engineering extended-connectivity fingerprints (ECFPs) to their molecular structures. *Chemical Science*, 11(38):10378–10389, October 2020. ISSN 2041-6539. doi: 10.1039/D0SC03115A. URL <https://pubs.rsc.org/en/content/articlelanding/2020/sc/d0sc03115a>. Publisher: The Royal Society of Chemistry.

Seul Lee, Jaehyeong Jo, and Sung Ju Hwang. Exploring Chemical Space with Score-based Out-of-distribution Generation. In *Proceedings of the 40th International Conference on Machine Learning*, pages 18872–18892. PMLR, July 2023. URL <https://proceedings.mlr.press/v202/lee23f.html>. ISSN: 2640-3498.

Seul Lee, Karsten Kreis, Srimukh Prasad Veccham, Meng Liu, Danny Reidenbach, Saeed Gopal Palival, Arash Vahdat, and Weili Nie. Molecule Generation with Fragment Retrieval Augmentation. In *The Thirty-eighth Annual Conference on Neural Information Processing Systems*, November 2024a. URL [https://openreview.net/forum?id=56Q0qggDlp&referrer=%5Bthe%20profile%20of%20Arash%20Vahdat%5D\(%2Fprofile%3Fid%3D~Arash_Vahdat3\)](https://openreview.net/forum?id=56Q0qggDlp&referrer=%5Bthe%20profile%20of%20Arash%20Vahdat%5D(%2Fprofile%3Fid%3D~Arash_Vahdat3)).

Seul Lee, Seanie Lee, Kenji Kawaguchi, and Sung Ju Hwang. Drug discovery with dynamic goal-aware fragments. In *International Conference on Machine Learning*, pages 26731–26751. PMLR, 2024b.

Yoav Levine, Noam Wies, Or Sharir, Hofit Bata, and Amnon Shashua. Limits to depth-efficiencies of self-attention. In *Proceedings of the 34th International Conference on Neural Information Processing Systems*, NIPS ’20, Red Hook, NY, USA, 2020. Curran Associates Inc. ISBN 9781713829546.

Anchen Li, Elena Casiraghi, and Juho Rousu. Chemical reaction enhanced graph learning for molecule representation. *Bioinformatics*, 40(10):btae558, October 2024. ISSN 1367-4811. doi: 10.1093/bioinformatics/btae558. URL <https://doi.org/10.1093/bioinformatics/btae558>.

Shuangli Li, Jingbo Zhou, Tong Xu, Dejing Dou, and Hui Xiong. GeomGCL: Geometric Graph Contrastive Learning for Molecular Property Prediction. *Proceedings of the AAAI Conference on Artificial Intelligence*, 36(4):4541–4549, June 2022. ISSN 2374-3468. doi: 10.1609/aaai.v36i4.20377. URL <https://ojs.aaai.org/index.php/AAAI/article/view/20377>. Number: 4.

Shitong Luo, Jiaqi Guan, Jianzhu Ma, and Jian Peng. A 3D generative model for structure-based drug design. In *Proceedings of the 35th International Conference on Neural Information Processing Systems*, NIPS ’21, pages 6229–6239, Red Hook, NY, USA, June 2024. Curran Associates Inc. ISBN 978-1-7138-4539-3.

Omar Mahmood, Elman Mansimov, Richard Bonneau, and Kyunghyun Cho. Masked graph modeling for molecule generation. *Nature Communications*, 12(1):3156, May 2021. ISSN 2041-1723. doi: 10.1038/s41467-021-23415-2. URL <https://www.nature.com/articles/s41467-021-23415-2>. Publisher: Nature Publishing Group.

Haggai Maron, Heli Ben-Hamu, Hadar Serviansky, and Yaron Lipman. Provably Powerful Graph Networks. In *Proceedings of the 33rd International Conference on Neural Information Processing Systems*, pages 2156–2167. Curran Associates Inc., Red Hook, NY, USA, December 2019.

Eyal Mazuz, Guy Shtar, Bracha Shapira, and Lior Rokach. Molecule generation using transformers and policy gradient reinforcement learning. *Scientific Reports*, 13(1):8799, May 2023. ISSN 2045-2322. doi: 10.1038/s41598-023-35648-w. URL <https://www.nature.com/articles/s41598-023-35648-w>. Number: 1 Publisher: Nature Publishing Group.

Christopher Morris, Martin Ritzert, Matthias Fey, William L. Hamilton, Jan Eric Lenssen, Gaurav Rattan, and Martin Grohe. Weisfeiler and Leman Go Neural: Higher-Order Graph Neural Networks. *Proceedings of the AAAI Conference on Artificial Intelligence*, 33(01):4602–4609, July 2019. ISSN 2374-3468. doi: 10.1609/aaai.v33i01.33014602. URL <https://ojs.aaai.org/index.php/AAAI/article/view/4384>. Number: 01.

Emmanuel Noutahi, Cristian Gabellini, Michael Craig, Jonathan S. C. Lim, and Prudencio Tossou. Gotta be SAFE: a new framework for molecular design. *Digital Discovery*, 3(4):796–804, 2024. doi: 10.1039/D4DD00019F. URL <https://pubs.rsc.org/en/content/articlelanding/2024/dd/d4dd00019f>. Publisher: Royal Society of Chemistry.

Noel O’Boyle and Andrew Dalke. DeepSMILES: An Adaptation of SMILES for Use in Machine-Learning of Chemical Structures, September 2018. URL <https://chemrxiv.org/engage/chemrxiv/article-details/60c73ed6567dfe7e5fec388d>.

Marcus Olivecrona, Thomas Blaschke, Ola Engkvist, and Hongming Chen. Molecular de-novo design through deep reinforcement learning. *Journal of Cheminformatics*, 9(1):48, September 2017. ISSN 1758-2946. doi: 10.1186/s13321-017-0235-x. URL <https://doi.org/10.1186/s13321-017-0235-x>.

Rıza Özçelik and Francesca Grisoni. The jungle of generative drug discovery: Traps, treasures, and ways out. *arXiv preprint arXiv:2501.05457*, 2024.

Marco Podda, Davide Bacci, and Alessio Micheli. A Deep Generative Model for Fragment-Based Molecule Generation. In *Proceedings of the Twenty Third International Conference on Artificial Intelligence and Statistics*, pages 2240–2250. PMLR, June 2020. URL <https://proceedings.mlr.press/v108/podda20a.html>. ISSN: 2640-3498.

Daniil Polykovskiy, Alexander Zhebrak, Benjamin Sanchez-Lengeling, Sergey Golovanov, Oktai Tatanov, Stanislav Belyaev, Rauf Kurbanov, Aleksey Artamonov, Vladimir Aladinskiy, Mark Veselov, Artur Kadurin, Simon Johansson, Hongming Chen, Sergey Nikolenko, Alán Aspuru-Guzik, and Alex Zhavoronkov. Molecular Sets (MOSES): A Benchmarking Platform for Molecular Generation Models. *Frontiers in Pharmacology*, 11, December 2020. ISSN 1663-9812. doi: 10.3389/fphar.2020.565644. URL <https://www.frontiersin.org/journals/pharmacology/articles/10.3389/fphar.2020.565644/full>. Publisher: Frontiers.

David Rogers and Mathew Hahn. Extended-Connectivity Fingerprints. *Journal of Chemical Information and Modeling*, 50(5):742–754, May 2010. ISSN 1549-9596. doi: 10.1021/ci100050t. URL <https://doi.org/10.1021/ci100050t>. Publisher: American Chemical Society.

Jerret Ross, Brian Belgodere, Vijil Chenthamarakshan, Inkit Padhi, Youssef Mroueh, and Payel Das. Large-Scale Chemical Language Representations Capture Molecular Structure and Properties, December 2022. URL <http://arxiv.org/abs/2106.09553>. arXiv:2106.09553 [cs, q-bio].

Jerret Ross, Brian Belgodere, Samuel C. Hoffman, Vijil Chenthamarakshan, Youssef Mroueh, and Payel Das. GP-MoLFormer: A Foundation Model For Molecular Generation, April 2024. URL <http://arxiv.org/abs/2405.04912>. arXiv:2405.04912 [q-bio].

Lars Ruddigkeit, Ruud van Deursen, Lorenz C. Blum, and Jean-Louis Reymond. Enumeration of 166 Billion Organic Small Molecules in the Chemical Universe Database GDB-17. *Journal of Chemical Information and Modeling*, 52(11):2864–2875, November 2012. ISSN 1549-9596. doi: 10.1021/ci300415d. URL <https://doi.org/10.1021/ci300415d>. Publisher: American Chemical Society.

John Schulman, Filip Wolski, Prafulla Dhariwal, Alec Radford, and Oleg Klimov. Proximal policy optimization algorithms. *arXiv preprint arXiv:1707.06347*, 2017.

Philippe Schwaller, Teodoro Laino, Théophile Gaudin, Peter Bolgar, Christopher A. Hunter, Costas Bekas, and Alpha A. Lee. Molecular Transformer: A Model for Uncertainty-Calibrated Chemical Reaction Prediction. *ACS Central Science*, 5(9):1572–1583, September 2019. ISSN 2374-7943. doi: 10.1021/acscentsci.9b00576. URL <https://doi.org/10.1021/acscentsci.9b00576>. Publisher: American Chemical Society.

Rico Sennrich, Barry Haddow, and Alexandra Birch. Neural Machine Translation of Rare Words with Subword Units. In Katrin Erk and Noah A. Smith, editors, *Proceedings of the 54th Annual Meeting of the Association for Computational Linguistics (Volume 1: Long Papers)*, pages 1715–1725, Berlin, Germany, August 2016. Association for Computational Linguistics. doi: 10.18653/v1/P16-1162. URL <https://aclanthology.org/P16-1162>.

Martin Simonovsky and Nikos Komodakis. GraphVAE: Towards Generation of Small Graphs Using Variational Autoencoders, February 2018. URL <http://arxiv.org/abs/1802.03480>. arXiv:1802.03480 [cs] version: 1.

Michael A Skinnider, R Greg Stacey, David S Wishart, and Leonard J Foster. Chemical language models enable navigation in sparsely populated chemical space. *Nature Machine Intelligence*, 3(9):759–770, 2021.

Jascha Sohl-Dickstein, Eric Weiss, Niru Maheswaranathan, and Surya Ganguli. Deep Unsupervised Learning using Nonequilibrium Thermodynamics. In *Proceedings of the 32nd International Conference on Machine Learning*, pages 2256–2265. PMLR, June 2015. URL <https://proceedings.mlr.press/v37/sohl-dickstein15.html>. ISSN: 1938-7228.

Ruslan N. Tazhigulov, Joshua Schiller, Jacob Oppenheim, and Max Winston. Molecular Fingerprints for Robust and Efficient ML-Driven Molecular Generation, November 2022. URL <http://arxiv.org/abs/2211.09086>. arXiv:2211.09086 [cs].

Morgan Thomas, Noel M O’Boyle, Andreas Bender, and Chris De Graaf. Augmented hill-climb increases reinforcement learning efficiency for language-based de novo molecule generation. *Journal of cheminformatics*, 14(1):68, 2022.

Morgan Thomas, Mazen Ahmad, Gary Tresadern, and Gianni De Fabritiis. Promptsmiles: prompting for scaffold decoration and fragment linking in chemical language models. *Journal of Cheminformatics*, 16(1):77, 2024.

Benjamin I. Tingle, Khanh G. Tang, Mar Castanon, John J. Gutierrez, Munkhzul Khurelbaatar, Chinzorig Dandarchuluun, Yurii S. Moroz, and John J. Irwin. ZINC-22-A Free Multi-Billion-Scale Database of Tangible Compounds for Ligand Discovery. *Journal of Chemical Information and Modeling*, 63(4):1166–1176, February 2023. ISSN 1549-9596. doi: 10.1021/acs.jcim.2c01253. URL <https://doi.org/10.1021/acs.jcim.2c01253>. Publisher: American Chemical Society.

Austin Tripp and José Miguel Hernández-Lobato. Genetic algorithms are strong baselines for molecule generation. *arXiv preprint arXiv:2310.09267*, 2023.

Ye Wang, Honggang Zhao, Simone Sciabola, and Wenlu Wang. cMolGPT: A Conditional Generative Pre-Trained Transformer for Target-Specific De Novo Molecular Generation. *Molecules*, 28(11):4430, January 2023. ISSN 1420-3049. doi: 10.3390/molecules28114430. URL <https://www.mdpi.com/1420-3049/28/11/4430>. Number: 11 Publisher: Multidisciplinary Digital Publishing Institute.

David Weininger. SMILES, a chemical language and information system. 1. Introduction to methodology and encoding rules. *Journal of Chemical Information and Computer Sciences*, 28(1):31–36, February 1988. ISSN 0095-2338. doi: 10.1021/ci00057a005. URL <https://doi.org/10.1021/ci00057a005>. Publisher: American Chemical Society.

Robin Winter, Floriane Montanari, Andreas Steffen, Hans Briem, Frank Noé, and Djork-Arné Clevert. Efficient multi-objective molecular optimization in a continuous latent space. *Chemical Science*, 10(34):8016–8024, August 2019. ISSN 2041-6539. doi: 10.1039/C9SC01928F. URL <https://pubs.rsc.org/en/content/articlelanding/2019/sc/c9sc01928f>. Publisher: The Royal Society of Chemistry.

Thomas Wolf, Lysandre Debut, Victor Sanh, Julien Chaumond, Clement Delangue, Anthony Moi, Pierrick Cistac, Tim Rault, Rémi Louf, Morgan Funtowicz, et al. Huggingface’s transformers: State-of-the-art natural language processing. *arXiv preprint arXiv:1910.03771*, 2019.

Zhenqin Wu, Bharath Ramsundar, Evan N Feinberg, Joseph Gomes, Caleb Geniesse, Aneesh S Pappu, Karl Leswing, and Vijay Pande. MoleculeNet: a benchmark for molecular machine learning. *Chemical science*, 9(2):513–530, 2018.

Jiacheng Xiong, Zhaoping Xiong, Kaixian Chen, Hualiang Jiang, and Mingyue Zheng. Graph neural networks for automated *de novo* drug design. *Drug Discovery Today*, 26(6):1382–1393, June 2021. ISSN 1359-6446. doi: 10.1016/j.drudis.2021.02.011. URL <https://www.sciencedirect.com/science/article/pii/S1359644621000787>.

Zhaoping Xiong, Dingyan Wang, Xiaohong Liu, Feisheng Zhong, Xiaozhe Wan, Xutong Li, Zhaojun Li, Xiaomin Luo, Kaixian Chen, Hualiang Jiang, and Mingyue Zheng. Pushing the Boundaries of Molecular Representation for Drug Discovery with the Graph Attention Mechanism. *Journal of Medicinal Chemistry*, 63(16):8749–8760, August 2020. ISSN 0022-2623. doi: 10.1021/acs.jmedchem.9b00959. URL <https://doi.org/10.1021/acs.jmedchem.9b00959>. Publisher: American Chemical Society.

Keyulu Xu*, Weihua Hu*, Jure Leskovec, and Stefanie Jegelka. How Powerful are Graph Neural Networks? In *International Conference on Learning Representations*, September 2018. URL <https://openreview.net/forum?id=ryGs6iA5Km>.

Minkai Xu, Alexander S. Powers, Ron O. Dror, Stefano Ermon, and Jure Leskovec. Geometric Latent Diffusion Models for 3D Molecule Generation. In *Proceedings of the 40th International Conference on Machine Learning*, pages 38592–38610. PMLR, July 2023. URL <https://proceedings.mlr.press/v202/xu23n.html>. ISSN: 2640-3498.

Soojung Yang, Doyeong Hwang, Seul Lee, Seongok Ryu, and Sung Ju Hwang. Hit and lead discovery with explorative rl and fragment-based molecule generation. *Advances in Neural Information Processing Systems*, 34:7924–7936, 2021.

Soojung Yang, Doyeong Hwang, Seul Lee, Seongok Ryu, and Sung Ju Hwang. Hit and lead discovery with explorative RL and fragment-based molecule generation. In *Proceedings of the 35th International Conference on Neural Information Processing Systems*, NIPS ’21, pages 7924–7936, Red Hook, NY, USA, June 2024. Curran Associates Inc. ISBN 978-1-7138-4539-3.

Botao Yu, Frazier N Baker, Ziqi Chen, Xia Ning, and Huan Sun. Llasmol: Advancing large language models for chemistry with a large-scale, comprehensive, high-quality instruction tuning dataset. In *First Conference on Language Modeling*, 2024.

Chengxi Zang and Fei Wang. MoFlow: An Invertible Flow Model for Generating Molecular Graphs. In *Proceedings of the 26th ACM SIGKDD International Conference on Knowledge Discovery & Data Mining*, KDD ’20, pages 617–626, New York, NY, USA, August 2020. Association for Computing Machinery. ISBN 978-1-4503-7998-4. doi: 10.1145/3394486.3403104. URL <https://dl.acm.org/doi/10.1145/3394486.3403104>.

Chuxu Zhang, Dongjin Song, Chao Huang, Ananthram Swami, and Nitesh V. Chawla. Heterogeneous Graph Neural Network. In *Proceedings of the 25th ACM SIGKDD International Conference on Knowledge Discovery & Data Mining*, KDD ’19, pages 793–803, New York, NY, USA, July 2019. Association for Computing Machinery. ISBN 978-1-4503-6201-6. doi: 10.1145/3292500.3330961. URL <https://dl.acm.org/doi/10.1145/3292500.3330961>.

Odin Zhang, Jintu Zhang, Jieyu Jin, Xujun Zhang, RenLing Hu, Chao Shen, Hanqun Cao, Hongyan Du, Yu Kang, Yafeng Deng, Furui Liu, Guangyong Chen, Chang-Yu Hsieh, and Tingjun Hou. ResGen is a pocket-aware 3D molecular generation model based on parallel multiscale modelling. *Nature Machine Intelligence*, 5(9):1020–1030, September 2023. ISSN 2522-5839. doi: 10.1038/s42256-023-00712-7. URL <https://www.nature.com/articles/s42256-023-00712-7>. Publisher: Nature Publishing Group.

Artem Zholus, Maksim Kuznetsov, Roman Schutski, Rim Shayakhmetov, Daniil Polykovskiy, Sarath Chandar, and Alex Zhavoronkov. BindGPT: A Scalable Framework for 3D Molecular Design via Language Modeling and Reinforcement Learning, June 2024. URL <http://arxiv.org/abs/2406.03686>. arXiv:2406.03686 [cs].

Gengmo Zhou, Zhifeng Gao, Qiankun Ding, Hang Zheng, Hongteng Xu, Zhewei Wei, Linfeng Zhang, and Guolin Ke. Uni-Mol: A Universal 3D Molecular Representation Learning Framework. In *The Eleventh International Conference on Learning Representations*, September 2022. URL <https://openreview.net/forum?id=6K2RM6wVqKu>.

A. Related Work

A.1. Representation of Molecules

Molecules are commonly depicted using structural diagrams, traditionally drawn with pen and paper, to represent bonds and atoms visually. However, in chem-informatics, more advanced representations are needed for the computational processing of molecular structures. In this context, "molecular representations" encompass any encoding of a chemical compound that can be employed for computational exploration of the chemical space. The current approaches to representing molecules can be broadly classified into four types: (i) Vector-based representations, (ii) Graph-based representations, (iii) 3D-based representations, and (iv) String-based representations.

Vector-based: Topological fingerprints, such as Extended Connectivity FingerPrints (ECFP) [Rogers and Hahn, 2010] and Molecular ACCess System (MACCS) [Durant et al., 2002], have traditionally been employed for substructure and molecule similarity searches. These fingerprints encode molecules as a sequence of bits in an identifier list, each denoting the presence or absence of a specific substructure. Although each molecular structure can be deterministically mapped to a fingerprint, the fingerprints are only partially invertible [Le et al., 2020], which limits their applicability in *de-novo* molecule generation [Gómez-Bombarelli et al., 2018, Tazhigulov et al., 2022]. Additionally, the fingerprints can be augmented with 2D molecular descriptors such as Molecular Weight, QED score, and Number of Aromatic Rings to help impose specific constraints on the generated molecules and make them more aligned with desired chemical properties or biological activity.

Graph-based: A 2D molecular graph is defined as $\mathcal{G} = (\mathcal{V}, \mathcal{E})$ where \mathcal{V} is the set of nodes (atoms) and \mathcal{E} is the set of edges (bonds). The type of atoms and edges can be represented using a feature matrix X . Graph Neural Networks (GNNs) have been used to learn the representations of molecules [Kipf and Welling, 2017, Xu* et al., 2018, Xiong et al., 2021] for tasks such as reaction prediction, property prediction and drug discovery. The initial frameworks for learning molecule representation used Message Passing Neural Networks (MPNNs) to compute the atom embedding based on neighbourhood information capturing local interaction effects [Gilmer et al., 2017]. Although many variants of GNNs have been proposed [Morris et al., 2019, Maron et al., 2019, Zhang et al., 2019, Brockschmidt, 2020, Xiong et al., 2020, Li et al., 2024], challenges remain in terms of higher-order expressivity, scalability, and computational cost.

3D-based: While using Graph Neural Networks (GNNs) on 2D molecular graphs is convenient and seem to be the obvious choice, the resulting representations often overlook crucial spatial information, such as the spatial direction and torsion angles between atoms [Guo et al., 2023]. Recent advancements in molecule representation learning have focused on integrating 3D coordinate information into 2D molecular graphs [Luo et al., 2024, Fang et al., 2022, Li et al., 2022]. Uni-Mol [Zhou et al., 2022] introduced a pretraining framework capable of directly utilizing 3D positions as inputs and outputs. However, a significant challenge in this approach is the existence of multiple low-energy conformations for a given molecule. These conformations are not easily accessible and are particularly difficult to compute, especially for large molecules and the vast chemical space, which spans billions of possible molecules.

String-based: 2D molecular structures can also be encoded as linear notations, which use specialized languages to represent molecular structures and compositions in chemistry. The earliest example of such a molecular language was developed in the 1980s by Weininger [1988]. The SMILES (Simplified Molecular Input Line Entry System) notation encodes atoms, bonds, and connectivity patterns using ASCII strings, where atoms are represented by characters (e.g., 'C' for carbon, 'N' for nitrogen) and bonds by special characters (e.g., '-' for a single bond, '=' for a double bond, '#' for a triple bond). However, the syntax rules and restrictive grammar of SMILES can result in many invalid molecules during parsing, even when the string appears to represent a plausible molecular structure. To address some of these limitations, DeepSMILES [O'Boyle and Dalke, 2018] was introduced, which avoids the issue of unbalanced parentheses by using only closing parentheses, where the number of parentheses indicates the branch length. More recently, SELFIES (Self-Referencing Embedded Strings) [Krenn et al., 2022] was developed as a linear notation that is 100% robust; every SELFIES string corresponds to a valid molecule, even for entirely random strings. Additionally, SAFE (Sequential Attachment-based Fragment Embedding) [Noutahi et al., 2024] introduced a framework for fragment-constrained molecule generation tasks while maintaining compatibility with existing SMILES parsers.

String-based molecular representations offer a computationally efficient and scalable approach to exploring the vast chemical space using unlabelled data without relying on additional information such as 3D geometry or complex optimization techniques. Despite their simplicity, these methods capture essential chemical information and structural features, making them valuable tools in computational chemistry and drug discovery.

A.2. Deep Generative Models for De-Novo Molecule Generation

Deep generative models have become a key approach for *de novo* molecule generation, facilitating the discovery of novel compounds by capturing complex patterns within the vast chemical space. Numerous methods have emerged, each focused on different molecular representations and assembly strategies [Olivecrona et al., 2017, Jin et al., 2018, Polykovskiy et al., 2020, Jin et al., 2020b, Bagal et al., 2022, Eckmann et al., 2022, Jo et al., 2022, Irwin et al., 2022, Fang et al., 2023, Lee et al., 2023, Yang et al., 2024, Ross et al., 2024].

Assembly Methods: Early approaches [Gómez-Bombarelli et al., 2018, Jin et al., 2018, Winter et al., 2019, Tazhigulov et al., 2022] primarily utilized Variational Autoencoders (VAEs) to transform SMILES representations into a continuous latent space, followed by sampling and decoding to generate discrete molecular structures. Graph-based generative models have emerged as a natural extension, directly leveraging the molecular graph structure where atoms are represented as nodes and bonds as edges [Cao and Kipf, 2022]. GraphVAE (Graph Variational Autoencoder) [Simonovsky and Komodakis, 2018] encodes and decodes molecules using edge-conditioned graph convolutions. MoFlow [Zang and Wang, 2020], a flow-based graph generative model learns invertible mappings between molecular graphs and their latent representations. Graph generation approaches utilize small molecular building blocks such as atoms and their performance degrades significantly for larger molecules. To tackle this problem recent works employ significantly larger and more flexible graph motifs as basic building blocks [Kuznetsov and Polykovskiy, 2021]. In parallel, 3D molecule generation has gained substantial attention, particularly through the use of diffusion models. G-Schnet [Gebauer et al., 2019], for instance, utilizes an autoregressive process to iteratively sample atoms and bonds in 3D space. Similarly, inspired by the success of diffusion models in other domains [Sohl-Dickstein et al., 2015, Ho et al., 2020, Kong et al., 2023], Hoogeboom et al. [2022] proposed an equivariant diffusion model for generating novel 3D molecular structures.

Optimization Methods: Molecule optimization involves navigating an immense and complex chemical space, which requires sophisticated algorithms capable of efficiently searching for and generating molecules with optimal characteristics. Several computational approaches have been developed to tackle this challenge, each with distinct mechanisms for exploring the design space and optimizing molecular properties. Reinforcement Learning treats molecule optimization as a sequential decision-making problem. In this context, the state typically represents a partially generated molecule, and actions correspond to modifications at the graph or string level. The reward function is based on the properties of the generated molecules, guiding the model toward desirable outcomes. Bayesian Optimization operates by learning a continuous latent space of molecular representations, optimizing target properties by navigating through this latent space. Genetic algorithms, inspired by natural evolutionary processes, explore the chemical space through operations such as mutation and crossover applied to a pool of candidate molecules, promoting diversity and exploration. Gradient ascent methods, on the other hand, estimate the gradient of a molecular property across the chemical space and use backpropagation to optimize molecular structures. Hill Climbing is an iterative optimization method with high-performing molecules from previous rounds incorporated into the training data to refine the generative model progressively.

While graph-based and 3D deep generative models have made significant strides in generating molecular structures, recent advances in natural language processing have opened new possibilities for *de novo* molecule generation and optimization. Large Language Models (LLMs) offer a novel approach for navigating the large chemical space, presenting new opportunities for optimizing molecular properties in a scalable and computationally feasible manner. Combining these models with traditional optimization techniques can further enhance the search for *de novo* molecules with desired properties, marking a significant step forward in drug discovery.

A.3. Language Models in Molecule Generation

LLMs can effectively model sequential data and have shown remarkable proficiency in understanding and generating human language [Dubey et al., 2024, Jiang et al., 2023, Groeneveld et al., 2024]. These architectures are now being repurposed to explore and generate molecular structures. When treated as sequences of tokens, 1D molecular representations inherently encode chemical information, including 2D bonding topology patterns, while LLMs further enhance this by learning to generate diverse molecular structures. These models leverage unlabelled molecular data from across the chemical space, offering a novel approach to *de novo* molecule generation and broadening the potential for chemical discovery. MolGPT [Bagal et al., 2022] employs a decoder-only transformer architecture, inspired by GPT, to predict SMILES token sequences for molecular generation. Building on these advancements, models like cMolGPT [Wang et al., 2023] have been developed to generate target-specific compounds by incorporating conditional training for property optimization. Taiga [Mazuz et al., 2023] extends this approach by employing a two-stage framework: first, the model treats molecular generation as a language modeling task by predicting the next token in SMILES strings. Subsequently, reinforcement learning (RL) is applied to optimize simple chemical properties such as QED (Quantitative Estimate of Drug-likeness) and logP (Octanol-Water Partition Coefficient). MolGen [Fang et al., 2023], in contrast, utilizes an encoder-decoder BART architecture, focusing on generating chemically valid molecules through the SELFIES notation. It incorporates a chemical feedback mechanism to align generative probabilities with real-world chemical preferences. SAFE-GPT [Noutahi et al., 2024] introduces a new line notation and trains a GPT-like model on 1.1 billion SAFE notations, demonstrating versatile and robust performance in both *de novo* and fragment-constrained molecule generation tasks.

Tokenizers, which convert raw text sequences into tokens, are a critical component of modern language models. In molecular language models, token vocabularies are often constructed using a predefined regular expression developed by Schwaller et al. [2019], which splits SMILES strings into relevant tokens representing each atom (e.g., 'C' for carbon, 'N' for nitrogen). Less commonly, subword tokenization algorithms such as Byte Pair Encoding (BPE) [Sennrich et al., 2016] or Unigram [Kudo, 2018] are employed, sometimes combined with atomwise pretokenization and BPE. Given that tokenizer design impacts every stage of the modeling pipeline, this study explores the effects of using learned tokenization methods versus hand-crafted approaches.

B. Dataset Diversity

To ensure the diversity of the dataset, we confirmed that it contains a broad range of molecular structures, which is crucial for generating a wide variety of valid, novel, and unique molecules. Figure B5 illustrates the diversity of the data. The left plot shows the distribution of molecular lengths, tokenized using an atomwise tokenizer, demonstrating variation in molecule size across batches. The right plot displays the Tanimoto similarity between molecule pairs, showcasing the structural diversity in each batch an essential factor for robust molecular generation.

C. Pretraining Configuration

Our pretraining experiments leverage the computational enhancements of the FlashAttention library [Dao et al., 2024], utilizing its Llama implementation within the HuggingFace Trainer framework ¹. Training was conducted in mixed precision mode using bfloat16 to maximize GPU efficiency. We adopted the AdamW optimizer with a learning rate of 6×10^{-4} , paired with a cosine learning rate scheduler. The scheduler includes a warmup phase of 2% of the total training steps, during which the learning rate linearly increases to its peak value of 6×10^{-4} before gradually decaying to a minimum of 6×10^{-5} .

To ensure consistency across experiments, we maintained a fixed global batch size of 19,200 molecules, with gradient accumulation and per-device batch size selected to fit within the memory constraints of 4 NVIDIA A100 GPUs (80 GB each). Weight decay was set to 0.01 to prevent overfitting, and gradient clipping was applied with a maximum gradient norm of 1.0. The AdamW optimizer used $\beta_1 = 0.9$ and $\beta_2 = 0.95$, ensuring stability during training. All experiments were conducted on a Linux cluster equipped with 64 CPU cores and

¹https://huggingface.co/docs/transformers/en/main_classes/trainer

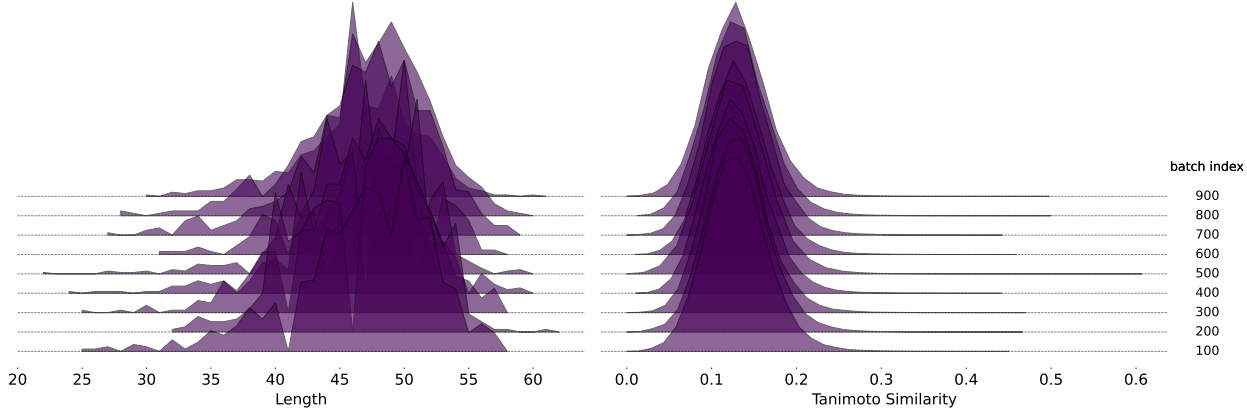


Figure B5: Diversity of the data across batches. The left plot shows the distribution of molecular lengths, tokenized using an atomwise tokenizer, indicating variation in molecule length within each batch. The right plot shows Tanimoto similarity between molecule pairs, demonstrating structural diversity in each batch.

512 GB of RAM. The architectural configurations for each model are summarized in Table C3.

Table C3: NovoMolGen Configurations

Components	NovoMolGen-32M	NovoMolGen-157M	NovoMolGen-300M
Attention Heads	8	10	12
Hidden Layers	12	24	32
Hidden Size	512	640	768
Intermediate Size	1024	2560	3072

D. Training curves

The training curves for various model sizes, tokenization strategies, and molecular representations are shown in Figures D6 to D9. Across model sizes (32M, 157M, 300M), we observe minimal difference in validation loss between random and scaffold-based splits for both the atomwise (Figure D6) and BPE (Figure D7) tokenizers, suggesting comparable performance under both evaluation strategies. Notably, in Figures D8 and D9, the DeepSMILES representation consistently achieves the lowest validation loss across both splits. Overall, models evaluated on the random split achieve slightly lower losses than those assessed on the scaffold split, indicating a modest challenge in generalizing to unseen scaffolds, although the performance gap remains small.

E. Fine-tuning Methodology

To optimize our models for goal-directed design, we performed a systematic hyperparameter search using a REINVENT-inspired Hill Climbing framework. The search was benchmarked across two distinct categories of tasks. For multi-property optimization, we used the **Perindopril_MPO** and **Zaleplon_MPO** tasks from the PMO benchmark. For protein-ligand docking, we used the **fa7** and **jak2** targets. Performance was evaluated by aggregating the sum of scores across all four settings. Each hyperparameter configuration was evaluated over three different random seeds, and the final score was averaged across seeds to mitigate variability.

The hyperparameter space explored includes the following:

- **Penalty Coefficient (λ):** [10, 100, 500, 2000]
- **Batch Size:** [32, 64]
- **Sigma (σ):** [500, 1000, 2000]

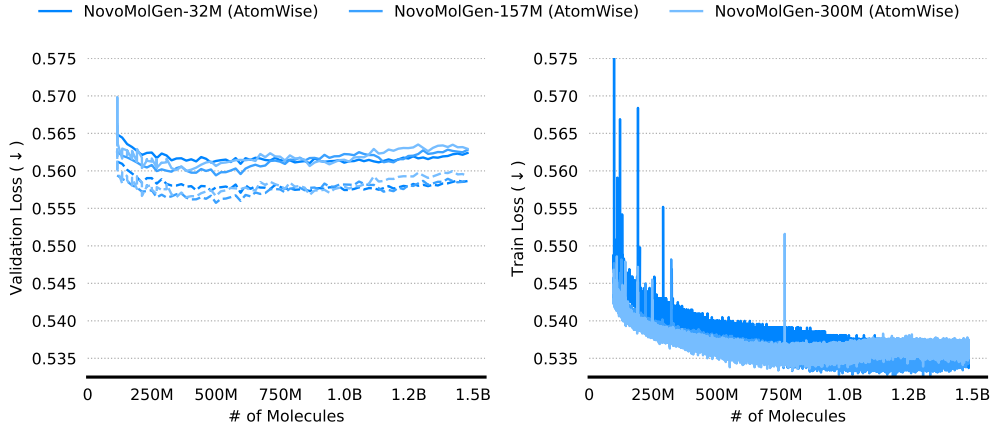


Figure D6: Training and validation loss curves for different model sizes. Solid lines denote performance on randomly split validation sets, while dashed lines indicate results on scaffold-split validation sets. The x-axis shows the number of molecules seen during training.

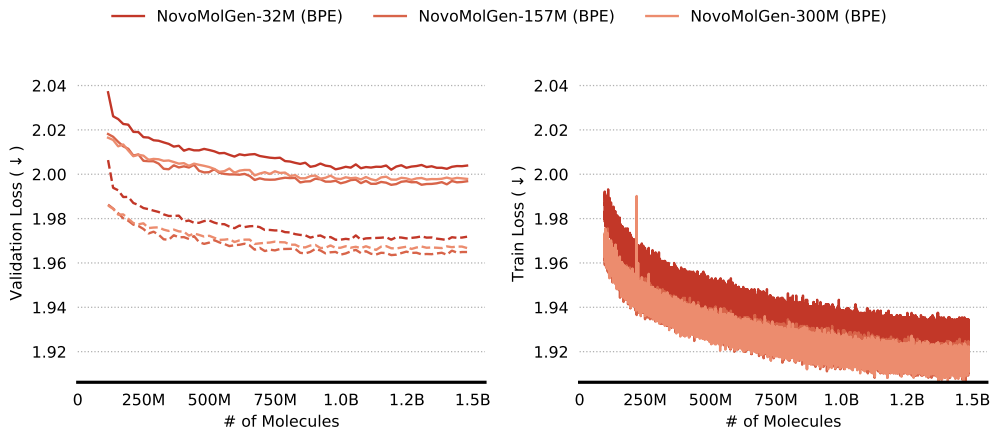


Figure D7: Training and validation loss curves for different model sizes with BPE tokenizer. Solid lines denote performance on randomly split validation sets, while dashed lines indicate results on scaffold-split validation sets. The x-axis shows the number of molecules seen during training.

- **Learning Rate (lr):** $[1 \times 10^{-3}, 5 \times 10^{-4}]$
- **Fraction of Top- k Molecules:** $[0.1, 0.5]$

The default value for penalty coefficient from the REINVENT implementation (5000) proved unsuitable for our models, likely due to differences in the log-likelihood scale of generated molecules, leading to unstable training and a high proportion of invalid solutions.

We conducted two separate hyperparameter searches to identify the optimal settings for each task category. For the PMO tasks, we evaluated numerous configurations on the **Perindopril_MPO** and **Zaleplon_MPO** benchmarks, selecting the best settings based on their aggregated score. A similar, independent hyperparameter search was performed for the protein-ligand docking tasks using the **fa7** and **jak2** targets. For statistical robustness, all evaluations in both searches were averaged over three independent random seeds. We evaluated 96 unique hyperparameter configurations, with each configuration run three times using different random seeds, totaling **576 experimental runs**. Our model could not generate any molecules for the **Valsartan_SMARTS** task, necessitating its exclusion from our analysis. This limitation stems directly from our choice of pre-training data, which lacks the specific chemical substructures required by the task's SMARTS pattern. We note that this is a data-dependent constraint, and other models may succeed where ours could not. For instance, a method

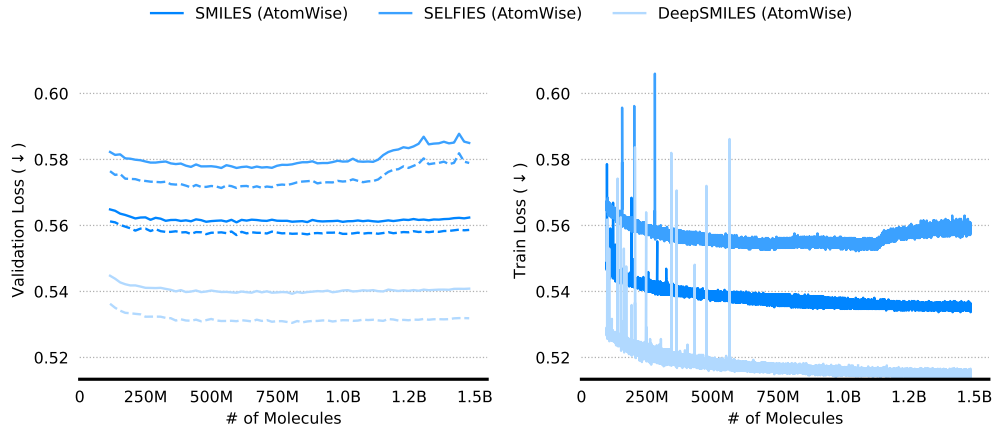


Figure D8: Training and validation loss curves for different molecule type with atomwise tokenizer. Solid lines denote performance on randomly split validation sets, while dashed lines indicate results on scaffold-split validation sets. The x-axis shows the number of molecules seen during training.

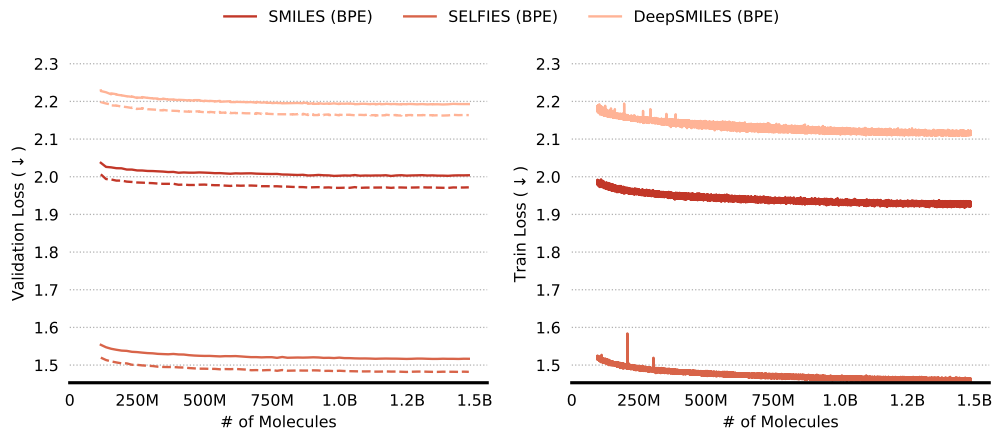


Figure D9: Training and validation loss curves for different molecule type with BPE tokenizer. Solid lines denote performance on randomly split validation sets, while dashed lines indicate results on scaffold-split validation sets. The x-axis shows the number of molecules seen during training.

like *f*-RAG , which builds its fragment vocabulary from the UniChem database, would likely be able to generate valid solutions provided that this database contains the relevant chemical motifs. The parallel coordinates plot are shown in Figures E10 to E21.

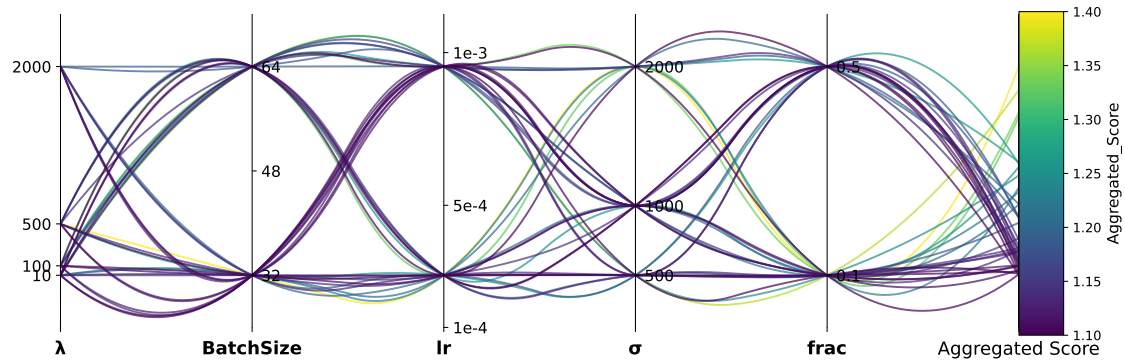


Figure E10: Parallel Coordinates Plot for the **SMILES (AtomWise)** model (32M), showing the importance and effects of hyperparameters on the Aggregated Score.

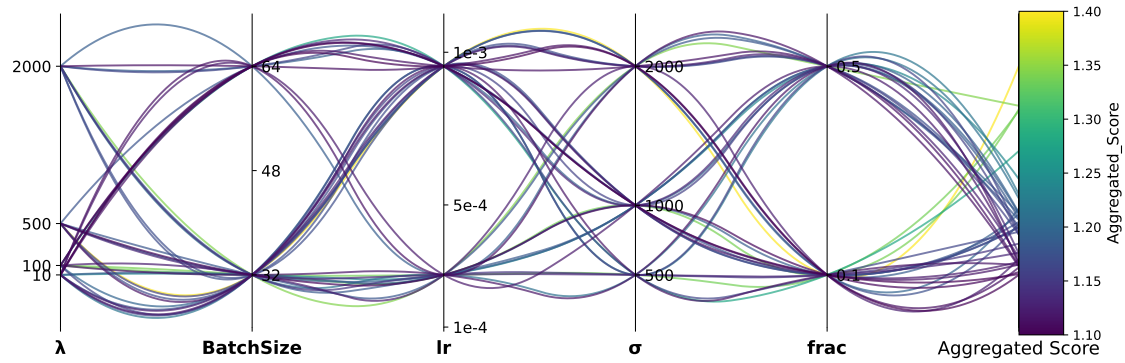


Figure E11: Parallel Coordinates Plot for the **SMILES (BPE)** model (32M).

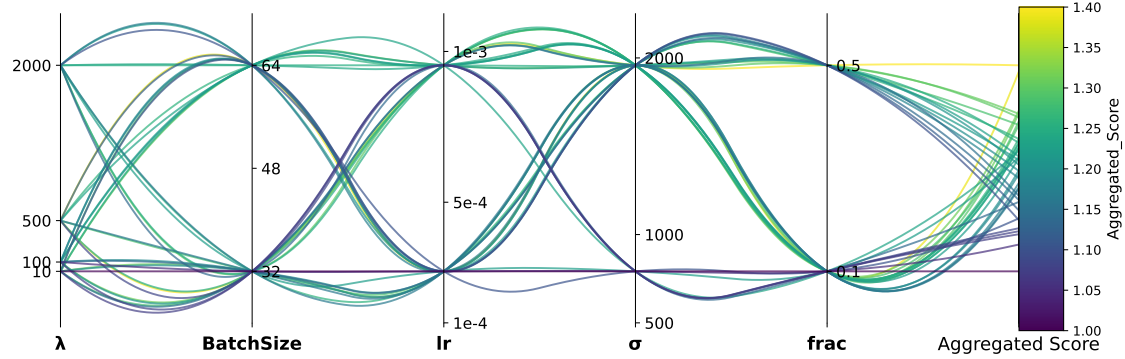


Figure E12: Parallel Coordinates Plot for the **SAFE (AtomWise)** model.

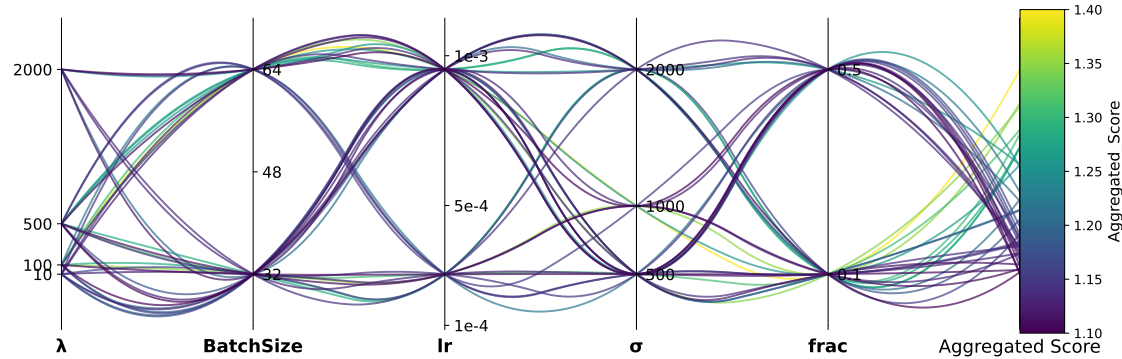


Figure E13: Parallel Coordinates Plot for the **SAFE (BPE)** model.

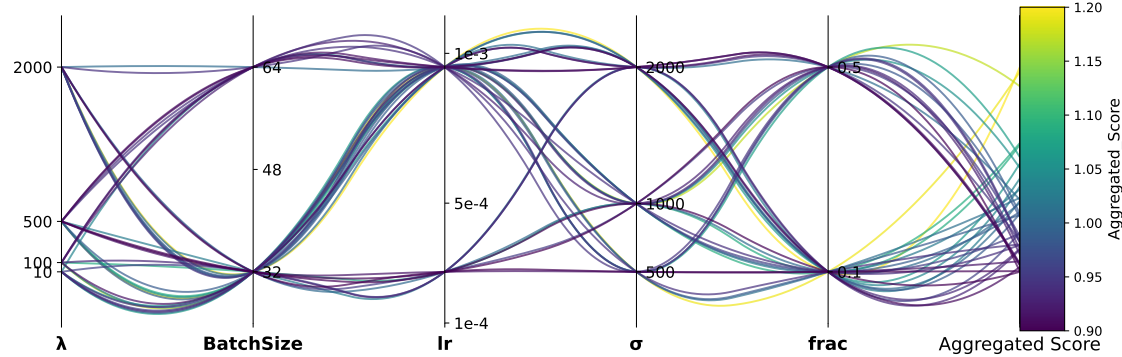


Figure E14: Parallel Coordinates Plot for the **SELFIES (AtomWise)** model.

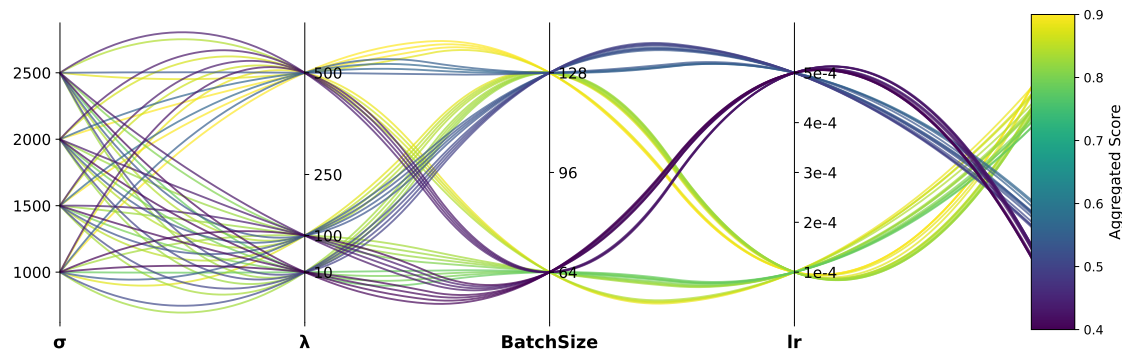


Figure E15: Parallel Coordinates Plot for the **SELFIES (BPE)** model.

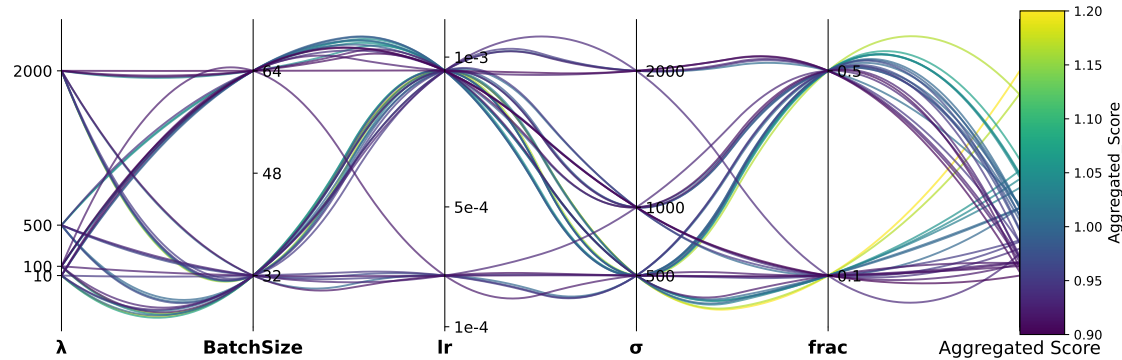


Figure E16: Parallel Coordinates Plot for the Deep SMILES (AtomWise) model.

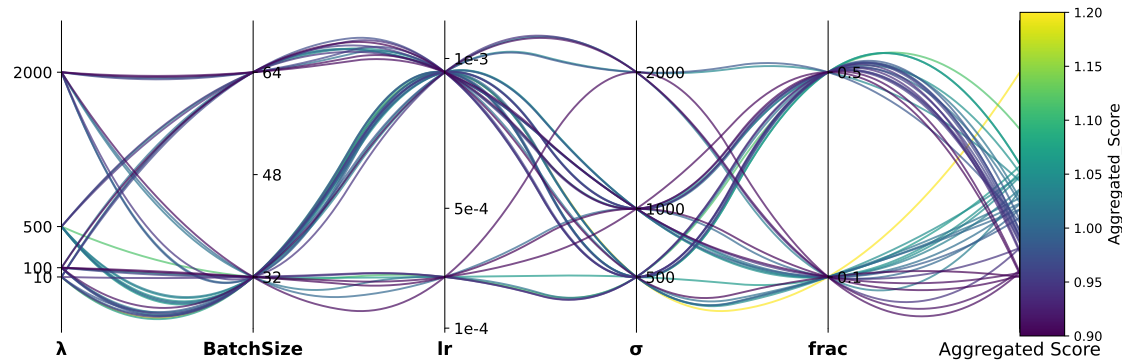


Figure E17: Parallel Coordinates Plot for the Deep SMILES (BPE) model.

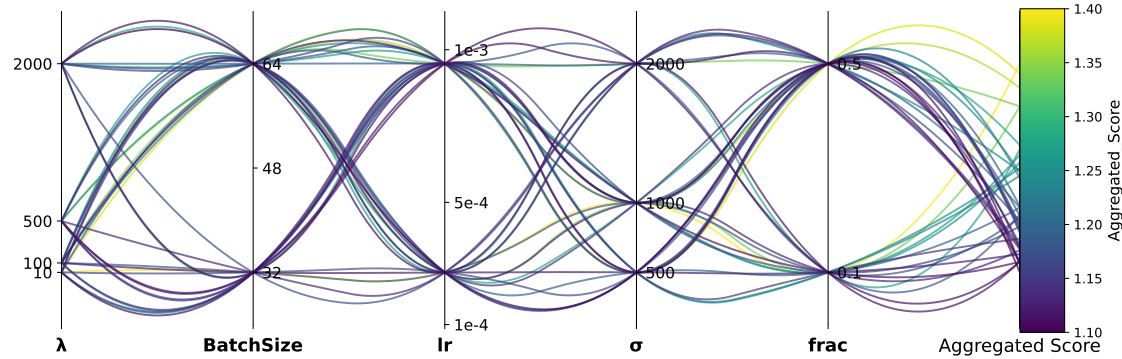


Figure E18: Parallel Coordinates Plot for the SMILES (AtomWise) model (157M).

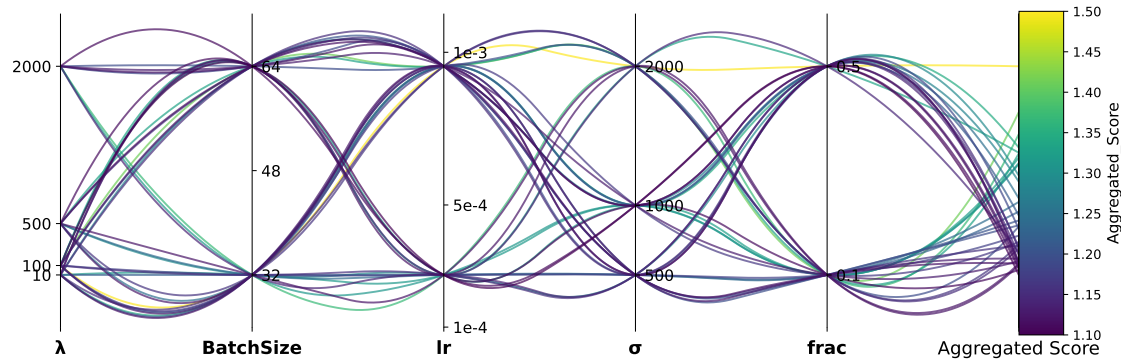


Figure E19: Parallel Coordinates Plot for the SMILES (BPE) model (157M).

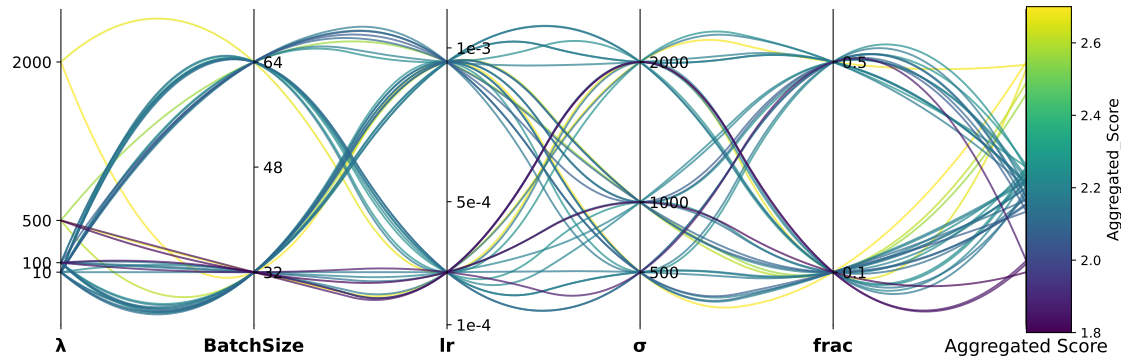


Figure E20: Parallel Coordinates Plot for the SMILES (AtomWise) model (300M).

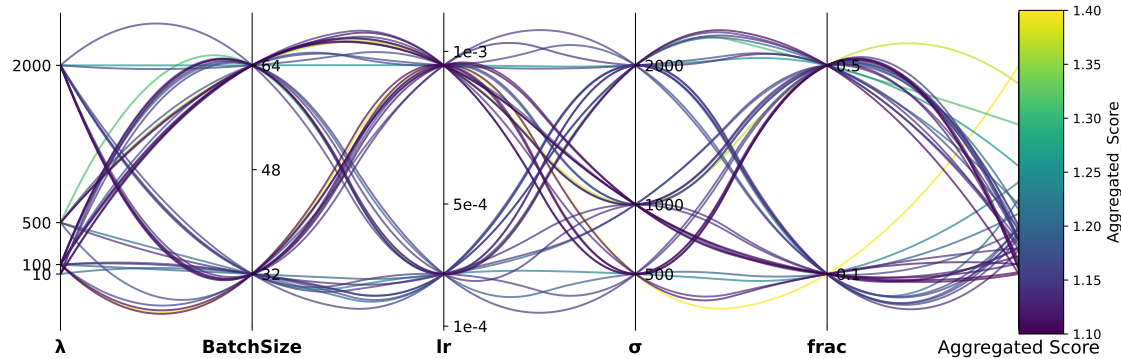


Figure E21: Parallel Coordinates Plot for the SMILES (BPE) model (300M).

F. Pretraining Metrics

This section describes the metrics used to assess the performance of our molecule generation model during pretraining, following the metrics outlined in the MOSES benchmark [Polykovskiy et al., 2020]. These metrics are computed based on the generated set of molecules from the model, denoted as G , and two reference sets: Test (ZINC-Random) and TestSF (ZINC-Scaffold), which correspond to molecules derived from a random split and a scaffold-based split, respectively. All reported metrics are calculated using the subset of G consisting of valid molecules identified through a post-generation filtering process except for validity.

1. **Validity:** Validity is determined using RDKit’s molecular structure parser, which verifies atomic valency and the consistency of bonds within aromatic rings. The metric ensures that the model adheres to relevant chemical constraints and measures the proportion of valid molecules generated within G . For molecular representations other than SMILES, we convert the generated set to SMILES and assess whether the corresponding decoder successfully decodes the molecule string to SMILES format. This step is essential, as representations that adhere to their respective syntactic rules may still produce chemically invalid molecules.
2. **Novelty:** This metric quantifies the proportion of molecules in G that do not appear in the training dataset. The molecules in G are canonicalized and compared against the training dataset, which comprises 1.5 billion molecules.
3. **Internal Diversity (IntDiv):** This metric quantifies the chemical diversity within a set of generated molecules (G). It is calculated by taking 1 minus the average pairwise Tanimoto similarity of the Morgan fingerprints for all molecules in the set. Higher IntDiv scores, which range from 0 (no diversity) to 1 (maximum diversity), indicate a more structurally varied set of generated molecules.
4. **Fréchet ChemNet Distance (FCD):** Derived from the activations of the penultimate layer of ChemNet, a deep neural network trained to predict the biological activities of drugs, this measure captures the chemical and biological properties of molecules. Activations for canonical SMILES representations of molecules are compared between the generated and reference sets. Lower values indicate better overlap, and the metric is non-negative.
5. **Fragment Similarity (Frag):** The distribution of BRICS fragments [Degen et al., 2008] is compared between the generated and reference sets. Higher values signify a closer match in fragment distributions, ensuring no fragment is disproportionately overrepresented or underrepresented.
6. **Scaffold Similarity (Scaff):** Similar to Fragment Similarity, this comparison uses Bemis-Murcko scaffolds instead of BRICS fragments to evaluate the resemblance between scaffolds in the generated and reference datasets.
7. **Similarity to Nearest Neighbor (SNN):** The average Tanimoto similarity between each molecule in the generated set and its nearest counterpart in the reference set is calculated. Lower values suggest the generated molecules are farther from the reference set’s manifold, while higher values indicate closer alignment.

G. Distribution Learning: Scaffold-based Validation Split

To ensure a fair comparison with baseline models [Polykovskiy et al., 2020, Jin et al., 2018, Eckmann et al., 2022, Fang et al., 2023], we report results for the generation of 30,000 molecules using held-out test sets of 175,000 molecules. All results are averaged over three independent model initialization seeds. Based on the results from Tables G4 to G6, NovoMolGen demonstrates state-of-the-art performance in terms of validity, novelty, and FCD scores. It performs comparably to other baselines on metrics related to fragments and scaffolds. Overall, the SMILES representation, across multiple model sizes and tokenization schemes, yields the best performance, although the differences among them are not substantial. SAFE underperforms in all metrics, with the exception of Internal Diversity. Furthermore, Byte Pair Encoding (BPE) emerges as the preferred tokenization strategy, outperforming atomwise for all the representations.

Table G4: Performance metrics for baseline models and **NovoMolGen** on Validity, Internal Diversity (IntDiv), and Novelty. Results are reported as mean_(std) over three independent model initializations. **Blue** denotes the best performing model, while **Pink** represents the second-best performing model (p value < 0.05).

REPRESENTATION	TOKENIZATION	MODEL SIZE	Valid (\uparrow)	IntDiv (\uparrow)	Novelty (\uparrow)
<i>Train</i>	–	–	1.000 _(0.0)	1.000 _(0.0)	0.0 _(0.0)
SMILES	GP-MOLFORMER [Ross et al., 2024]	ATOMWISE	46.8M	1.000	0.865
		ATOMWISE	32M	0.999 _(0.0001)	0.851 _(0.0001) 0.983 _(0.0001)
		ATOMWISE	157M	0.999 _(0.0001)	0.851 _(0.0001) 0.981 _(0.0001)
	SELFIES	ATOMWISE	300M	0.999 _(0.0001)	0.851 _(0.0001) 0.981 _(0.0001)
		BPE	32M	0.999 _(0.0001)	0.851 _(0.0001) 0.982 _(0.0001)
		BPE	157M	0.999 _(0.0001)	0.852 _(0.0001) 0.980 _(0.0001)
		BPE	300M	0.999 _(0.0001)	0.851 _(0.0000) 0.979 _(0.0001)
	DEEPSMILES	ATOMWISE	32M	1.000 _(0.0000)	0.852 _(0.0002) 0.982 _(0.0001)
		BPE	32M	1.000 _(0.0000)	0.851 _(0.0000) 0.984 _(0.0001)
SAFE	ATOMWISE	32M	0.957 _(0.0012)	0.853 _(0.0001)	0.953 _(0.0001)
		BPE	32M	0.997 _(0.0007)	0.852 _(0.0001) 0.976 _(0.0001)

Table G5: Performance metrics for baseline models and **NovoMolGen** on Fréchet ChemNet Distance (FCD) and Similarity to Nearest Neighbor (SNN). Results are presented for both the random validation set (Test) and scaffold-split validation set (TestSF), with values reported as mean_(std) over three independent model initializations. **Blue** denotes the best performing model, while **Pink** represents the second-best performing model (p value < 0.05). The baselines for CharRNN, VAE, and JT-VAE are sourced from Polykovskiy et al. [2020], while the results for LIMO, MolGen-7b, and GP-Molformer are taken from Ross et al. [2024].

REPRESENTATION	TOKENIZATION	MODEL SIZE	FCD (\downarrow)		SNN (\uparrow)	
			Test	TestSF	Test	TestSF
<i>Train</i>	–	–	0.0376 _(0.0002)	0.2392 _(0.01)	0.4657 _(0.0001)	0.4550 _(0.0001)
SMILES	CHARRNN [Polykovskiy et al., 2020]	ATOMWISE	–	0.0732 _(0.0247)	0.5204 _(0.0379)	0.6015 _(0.0206) 0.5649 _(0.0142)
		ATOMWISE	–	0.0990 _(0.0125)	0.5670 _(0.0338)	0.6257 _(0.0005) 0.5783 _(0.0008)
		ATOMWISE	–	0.3954 _(0.0234)	0.9382 _(0.0531)	0.5477 _(0.0076) 0.5194 _(0.007)
	VAE [Polykovskiy et al., 2020]	ATOMWISE	–	26.78	–	0.2464
		ATOMWISE	7B	0.0435	–	0.5138
		ATOMWISE	46.8M	0.0591	–	0.5045
	JT-VAE [Jin et al., 2018]	ATOMWISE	32M	0.0394 _(0.0002)	0.2386 _(0.0039)	0.4657 _(0.0002) 0.4551 _(0.0001)
		ATOMWISE	157M	0.0426 _(0.0012)	0.2225 _(0.0006)	0.4656 _(0.0002) 0.4551 _(0.0001)
		ATOMWISE	300M	0.0419 _(0.0004)	0.2446 _(0.0074)	0.4657 _(0.0001) 0.4548 _(0.0001)
SELFIES	LIMO [Eckmann et al., 2022]	ATOMWISE	32M	0.0384 _(0.0008)	0.2402 _(0.0045)	0.4654 _(0.0003) 0.4550 _(0.0001)
		ATOMWISE	157M	0.0384 _(0.0008)	0.2404 _(0.0034)	0.4655 _(0.0003) 0.4547 _(0.0001)
	MOLGEN-7B [Fang et al., 2023]	ATOMWISE	32M	0.0380 _(0.0003)	0.2463 _(0.0125)	0.4657 _(0.0003) 0.4550 _(0.0002)
		ATOMWISE	32M	0.0799 _(0.0031)	0.2480 _(0.0032)	0.4651 _(0.0003) 0.4549 _(0.0002)
DEEPSMILES	ATOMWISE	32M	0.0400 _(0.0006)	0.2504 _(0.0018)	0.4661 _(0.0001) 0.4554 _(0.0002)	
	BPE	32M	0.0380 _(0.0004)	0.2390 _(0.0048)	0.4655 _(0.0001) 0.4546 _(0.0002)	
SAFE	ATOMWISE	32M	0.9475 _(0.0042)	1.1979 _(0.0106)	0.4562 _(0.0001) 0.4459 _(0.0003)	
	BPE	32M	0.3283 _(0.0045)	0.5506 _(0.0004)	0.4599 _(0.0002) 0.4492 _(0.0003)	

Table G6: Performance metrics for baseline models and **NovoMolGen** on Fragment similarity (Frag) and Scaffold similarity (Scaf). Results are presented for both the random validation set (Test) and scaffold-split validation set (TestSF), with values reported as mean_(std) over three independent model initializations. **Blue** denotes the best performing model, while **Pink** represents the second-best performing model (p value < 0.05). The baselines for CharRNN, VAE, and JT-VAE are sourced from Polykovskiy et al. [2020], while the results for LIMO, MolGen-7b, and GP-Molformer are taken from Ross et al. [2024].

REPRESENTATION	TOKENIZATION	MODEL SIZE	Frag (\uparrow)		Scaf (\uparrow)	
			Test	TestSF	Test	TestSF
<i>Train</i>	–	–	0.9999 _(0.00006)	0.9974 _(0.0001)	0.5144 _(0.005)	0.0 _(0.0)
CHARRNN [Polykovskiy et al., 2020]	ATOMWISE	–	0.9998_(0.0002)	0.9983 _(0.0003)	0.9242_(0.0058)	0.1101_(0.0081)
VAE [Polykovskiy et al., 2020]	ATOMWISE	–	0.9994 _(0.0001)	0.9984_(0.0003)	0.9386_(0.0021)	0.0588 _(0.0095)
JT-VAE [Jin et al., 2018]	ATOMWISE	–	0.9965 _(0.0003)	0.9947 _(0.0002)	0.8964 _(0.0039)	0.1009_(0.0105)
LIMO [Eckmann et al., 2022]	ATOMWISE	–	0.6989	–	0.0079	–
MOLGEN-7B [Fang et al., 2023]	ATOMWISE	7B	0.9999	–	0.6538	–
GP-MOLFORMER [Ross et al., 2024]	ATOMWISE	46.8M	0.9998	–	0.7383	–
SMILES	ATOMWISE	32M	0.9999_(0.0000)	0.9977 _(0.0001)	0.5309 _(0.0022)	0.0091 _(0.0023)
		157M	0.9999_(0.0000)	0.9980_(0.0001)	0.5200 _(0.0045)	0.0095 _(0.0036)
		300M	0.9999_(0.0000)	0.9973 _(0.0002)	0.5219 _(0.0136)	0.0065 _(0.0009)
	BPE	32M	0.9999_(0.0000)	0.9974 _(0.0001)	0.5182 _(0.0126)	0.0098 _(0.0013)
		157M	0.9999_(0.0000)	0.9974 _(0.0001)	0.5193 _(0.0099)	0.0114 _(0.0036)
		300M	0.9999_(0.0000)	0.9974 _(0.0001)	0.5173 _(0.0094)	0.0131 _(0.0023)
SELFIES	ATOMWISE	32M	0.9996 _(0.0000)	0.9977 _(0.0000)	0.4765 _(0.0066)	0.0071 _(0.0005)
	BPE	32M	0.9999_(0.0000)	0.9973 _(0.0002)	0.5105 _(0.0133)	0.0061 _(0.0028)
DEEPSMILES	ATOMWISE	32M	0.9999_(0.0000)	0.9974 _(0.0000)	0.5218 _(0.0080)	0.0098 _(0.0044)
	BPE	32M	0.9999_(0.0000)	0.9973 _(0.0001)	0.5165 _(0.0008)	0.0070 _(0.0032)
SAFE	ATOMWISE	32M	0.9955 _(0.0001)	0.9936 _(0.0002)	0.4521 _(0.0137)	0.0094 _(0.0019)
	BPE	32M	0.9972 _(0.0000)	0.9946 _(0.0002)	0.4913 _(0.0014)	0.0059 _(0.0028)

H. Property Distributions

The distribution of properties serves as a valuable tool for visually evaluating the generated structures. We present a kernel density estimation of these distributions and calculate the Wasserstein-1 distance to compare the distributions of the generated and reference datasets. We use the following properties:

1. **Quantitative Estimation of Drug-likeness (QED):** A metric derived from medicinal chemistry principles that quantifies the drug-likeness of molecules on a scale from 0 to 1.
2. **Synthetic Accessibility (SA):** A measure of a molecule's synthesizability, calculated based on the contributions of molecular fragments. The metric ranges from 10 (difficult to synthesize) to 2 (easily synthesizable).
3. **Octanol-Water Partition Coefficient (logP):** Represents the ratio of a compound's concentration in the octanol phase to its concentration in the aqueous phase in a two-phase octanol/water system, serving as an indicator of solubility.
4. **Molecular Weight (MW):** Evaluates whether the generated set is biased toward heavier or lighter molecules, computed as the sum of atomic weights.
5. **Topological Polar Surface Area (TPSA):** Estimated based on functional group contributions from a database of substructures, this metric reflects lipid solubility and molecular polarity. Higher TPSA values indicate reduced absorption and distribution within the body.
6. **Bertz Complexity:** A graph-theoretical measure that quantifies molecular complexity using structural invariants and information-theoretic principles.
7. **Number of Rings (NumRings) and Rotatable Bonds:** Represents the number of independent closed-ring structures and rotatable bonds within a molecule, which are essential for analyzing molecular topology and are commonly used in cheminformatics for compound classification and comparison.

The kernel density estimation plots in Figure H22 indicate that NovoMolGen successfully generates molecules whose property distributions align closely with those of both the training dataset and the scaffold-split dataset. Additionally, a lower Wasserstein-1 distance is observed across all properties, further demonstrating the model's ability to replicate the reference distributions. The training dataset contains a higher proportion of molecules with favorable drug-like properties, including higher drug-likeness scores ($\text{QED} > 0.6$), greater synthetic accessibility ($\text{SA} < 4$), optimal solubility ($1 < \text{logP} < 4$), and an ideal molecular weight range ($300 < \text{MW} < 500$). By closely matching this distribution, NovoMolGen generates molecules with an increased likelihood of exhibiting drug-like characteristics. Furthermore, the model effectively captures molecular topology, as reflected in the distributions of NumRings, Rotatable Bonds, and Bertz Complexity. These results highlight the potential of NovoMolGen in generating chemically relevant and synthetically accessible molecules suitable for drug discovery applications.



Figure H22: Distributions of molecular properties for reference sets (ZINC-Random and ZINC-Scaffold, 175,000 molecules each) and a generated set from **NovoMolGen-SMILES-BPE-32M** (100,000 molecules). The properties include QED, SA, logP, MW, TPSA, Bertz Complexity, number of rotatable bonds, and number of rings.

I. PMO Benchmark

This appendix provides a comprehensive analysis of the PMO benchmark results for **NovoMolGen**, assessing its performance across varying model sizes, tokenization strategies, and intermediate training checkpoints. In Figure I23, the results are presented, highlighting the influence of model size and tokenization approaches on

the performance of NovoMolGen. Additionally, Figure I24 tracks the performance progression of NovoMolGen-32M-Atomwise across intermediate checkpoints, demonstrating the evolution of model performance with the optimal hyperparameter configuration and atomwise tokenization. The evaluation includes comparisons with the REINVENT and *f*-RAG baselines, with the mean and standard deviation of 3 independent runs presented in Tables I7 and I8. The reward curve for MPO tasks is shown in Figure I26.

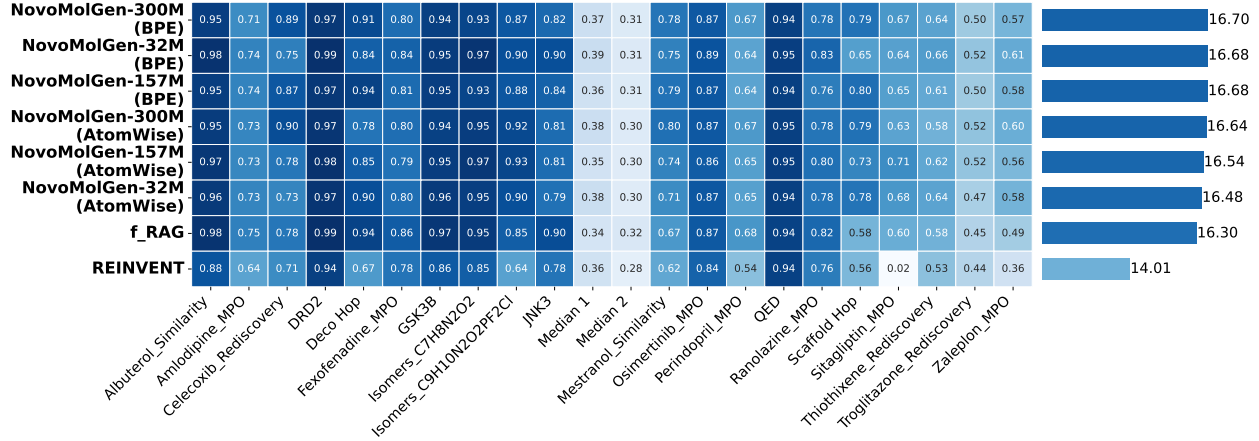


Figure I23: PMO benchmark results for **NovoMolGen-SMILES-32M** across model sizes and tokenization strategies. The **heatmap** (left) shows normalized scores per task, while the **bar chart** (right) presents total scores (higher is better). Baselines are REINVENT and *f*-RAG .

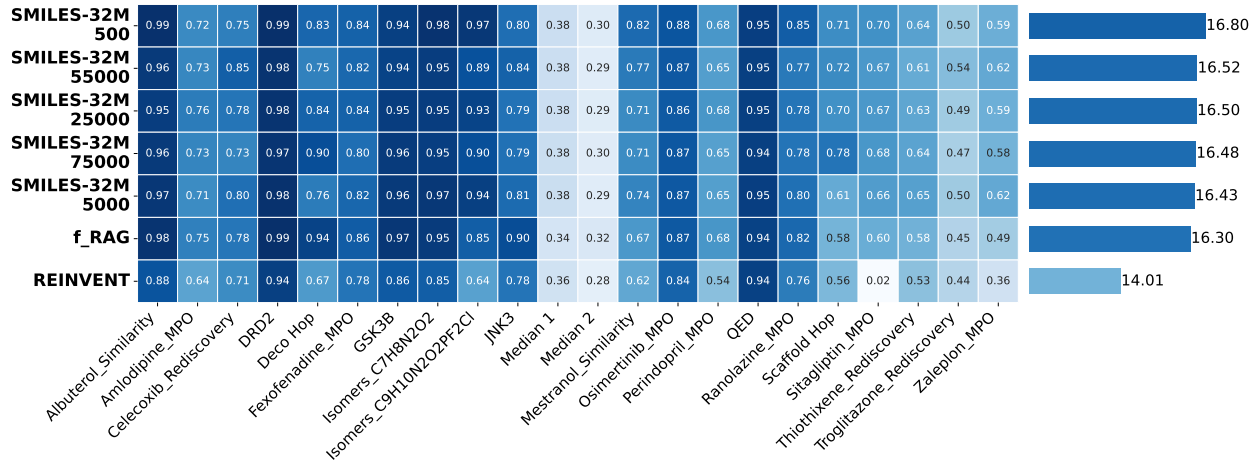


Figure I24: PMO benchmark results for intermediate checkpoints for **NovoMolGen-SMILES-32M** (best hyperparameter configuration, atomwise tokenization). The **heatmap** (left) shows normalized scores per task, while the **bar chart** (right) presents total scores (higher is better). Baselines are REINVENT and *f*-RAG .

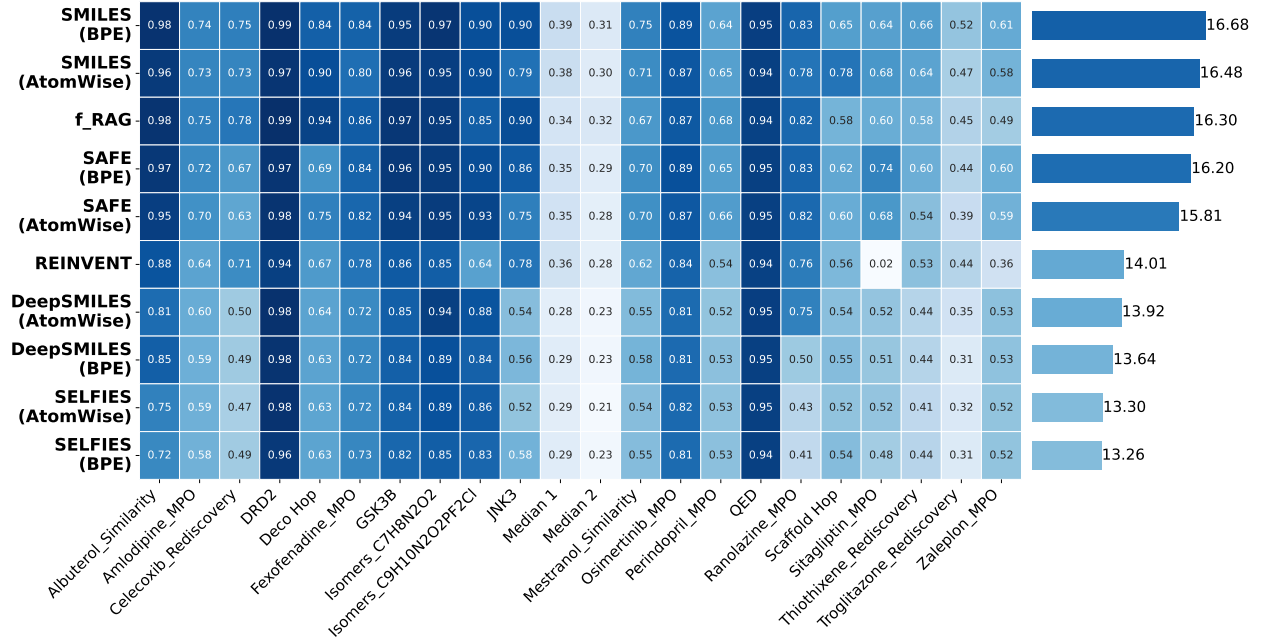


Figure I25: PMO benchmark results for all molecule types **NovoMolGen-32M**. The **heatmap** (left) shows normalized scores per task, while the **bar chart** (right) presents total scores (higher is better). Baselines are REINVENT and *f*-RAG.

Table I7: PMO AUC Top-10 results. Results are reported as mean_(std) over three independent model initializations for **SMILES** molecule type. **Blue** denotes the best performing model, while **Pink** represents the second-best performing model (*p* value < 0.05).

Oracle	<i>f</i> -RAG	REINVENT	NovoMolGen-32M (AtomWise)	NovoMolGen-157M (AtomWise)	NovoMolGen-300M (AtomWise)
albuterol_similarity	0.977 (0.002)	0.882(0.006)	0.958(0.003)	0.968 (0.002)	0.954(0.002)
amlodipine_mpo	0.749 (0.019)	0.635(0.035)	0.732 (0.024)	0.730(0.037)	0.730(0.007)
celecoxib_rediscovery	0.778 (0.007)	0.713(0.067)	0.732(0.009)	0.777(0.132)	0.904 (0.022)
drd2	0.936(0.011)	0.666(0.044)	0.973 (0.001)	0.983 (0.002)	0.972(0.001)
deco_hop	0.992 (0.000)	0.945 (0.007)	0.902(0.007)	0.853(0.115)	0.785(0.130)
fexofenadine_mpo	0.856 (0.016)	0.784(0.006)	0.802(0.008)	0.790(0.028)	0.803 (0.018)
gsk3b	0.969 (0.003)	0.865(0.043)	0.955 (0.006)	0.949(0.005)	0.941(0.012)
isomers_c7h8n2o2	0.955 (0.008)	0.852(0.036)	0.961(0.001)	0.965 (0.002)	0.949(0.005)
isomers_c9h10n2o2pf2cl	0.850(0.005)	0.642(0.054)	0.898(0.032)	0.926 (0.024)	0.915 (0.022)
jnk3	0.904 (0.004)	0.783(0.023)	0.787(0.014)	0.809 (0.066)	0.808(0.045)
median1	0.340(0.007)	0.356(0.009)	0.380 (0.003)	0.354(0.027)	0.379 (0.002)
median2	0.323 (0.005)	0.276(0.008)	0.300(0.013)	0.299(0.001)	0.304 (0.019)
mestranol_similarity	0.671(0.021)	0.618(0.048)	0.712(0.047)	0.739 (0.068)	0.796 (0.046)
osimertinib_mpo	0.866(0.009)	0.837(0.009)	0.874 (0.013)	0.858(0.001)	0.871 (0.011)
perindopril_mpo	0.681 (0.017)	0.537(0.016)	0.637(0.050)	0.649(0.037)	0.668 (0.011)
qed	0.939(0.001)	0.941(0.000)	0.945(0.000)	0.946 (0.000)	0.945 (0.000)
ranolazine_mpo	0.820 (0.016)	0.760(0.009)	0.784(0.007)	0.797 (0.023)	0.779(0.024)
scaffold_hop	0.576(0.014)	0.560(0.019)	0.783 (0.123)	0.735(0.140)	0.791 (0.160)
sitagliptin_mpo	0.601(0.011)	0.021(0.009)	0.677 (0.018)	0.708 (0.038)	0.635(0.043)
thiothixene_rediscovery	0.584(0.009)	0.534(0.013)	0.635 (0.018)	0.624 (0.050)	0.584(0.062)
troglitazone_rediscovery	0.448(0.017)	0.441(0.032)	0.470(0.042)	0.516 (0.010)	0.524 (0.058)
zaleplon_mpo	0.486(0.004)	0.358(0.062)	0.579 (0.023)	0.559(0.013)	0.599 (0.000)
Sum	16.30	14.01	16.48	16.54	16.64

Table I8: PMO AUC Top-10 results. Results are reported as $\text{mean}_{(\text{std})}$ over three independent model initializations for SMILES molecule type. **Blue** denotes the best performing model, while **Pink** represents the second-best performing model (p value < 0.05).

Oracle	f-RAG	REINVENT	NovoMolGen-32M (BPE)	NovoMolGen-157M (BPE)	NovoMolGen-300M (BPE)
albuterol_similarity	0.977 (0.002)	0.882(0.006)	0.981 (0.001)	0.951(0.000)	0.949(0.001)
amlodipine_mpo	0.749 (0.019)	0.635(0.035)	0.739 (0.021)	0.739(0.026)	0.713(0.010)
celecoxib_rediscovery	0.778(0.007)	0.713(0.067)	0.751(0.190)	0.872 (0.061)	0.890 (0.018)
drd2	0.936(0.011)	0.666(0.044)	0.987 (0.001)	0.967(0.001)	0.967 (0.000)
deco_hop	0.992 (0.000)	0.945 (0.007)	0.844(0.121)	0.937(0.008)	0.914(0.051)
fexofenadine_mpo	0.856 (0.016)	0.784(0.006)	0.837 (0.022)	0.810(0.012)	0.804(0.002)
gsk3b	0.969 (0.003)	0.865(0.043)	0.953 (0.013)	0.947(0.000)	0.944(0.006)
isomers_c7h8n2o2	0.955 (0.008)	0.852(0.036)	0.975 (0.003)	0.929(0.006)	0.928(0.006)
isomers_c9h10n2o2pf2cl	0.850(0.005)	0.642(0.054)	0.897 (0.027)	0.876 (0.005)	0.874(0.011)
jnk3	0.904 (0.004)	0.783(0.023)	0.899 (0.049)	0.839(0.044)	0.818(0.025)
median1	0.340(0.007)	0.356(0.009)	0.388 (0.003)	0.364(0.013)	0.374 (0.002)
median2	0.323 (0.005)	0.276(0.008)	0.310 (0.031)	0.305(0.016)	0.307(0.021)
mestranol_similarity	0.671(0.021)	0.618(0.048)	0.745(0.028)	0.789 (0.018)	0.780 (0.040)
osimertinib_mpo	0.866(0.009)	0.837(0.009)	0.885 (0.012)	0.873 (0.008)	0.870(0.008)
perindopril_mpo	0.681 (0.017)	0.537(0.016)	0.635(0.018)	0.636(0.036)	0.669 (0.049)
qed	0.939(0.001)	0.941(0.000)	0.947 (0.000)	0.945(0.000)	0.945 (0.000)
ranolazine_mpo	0.820 (0.016)	0.760(0.009)	0.830 (0.010)	0.760(0.018)	0.780(0.012)
scaffold_hop	0.576(0.014)	0.560(0.019)	0.650(0.002)	0.803 (0.063)	0.790 (0.134)
sitagliptin_mpo	0.601(0.011)	0.021(0.009)	0.643(0.034)	0.650 (0.040)	0.673 (0.044)
thiothixene_rediscovery	0.584(0.009)	0.534(0.013)	0.657 (0.012)	0.615 (0.010)	0.638(0.003)
troglitazone_rediscovery	0.448(0.017)	0.441(0.032)	0.517 (0.032)	0.497 (0.016)	0.496(0.003)
zaleplon_mpo	0.486(0.004)	0.358(0.062)	0.611 (0.027)	0.578 (0.041)	0.574(0.010)
Sum	16.30	14.01	16.68	16.68	16.70

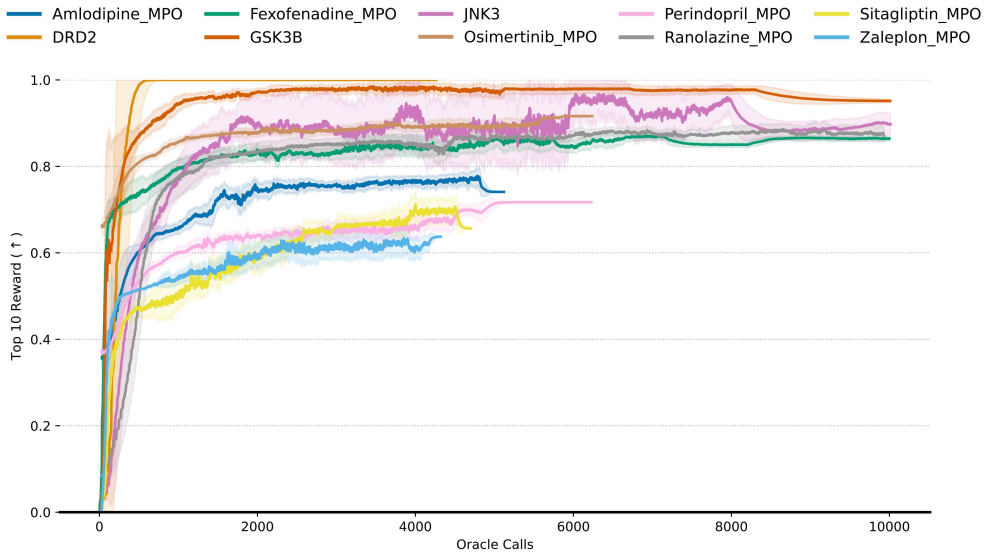


Figure I26: Sample efficiency of NovoMolGen-SMILES-BPE-32M on goal-directed generation tasks from PMO benchmark. The plot tracks the top 10 reward of the reward distribution as a function of oracle calls, demonstrating our model’s ability to rapidly discover high-reward molecules.

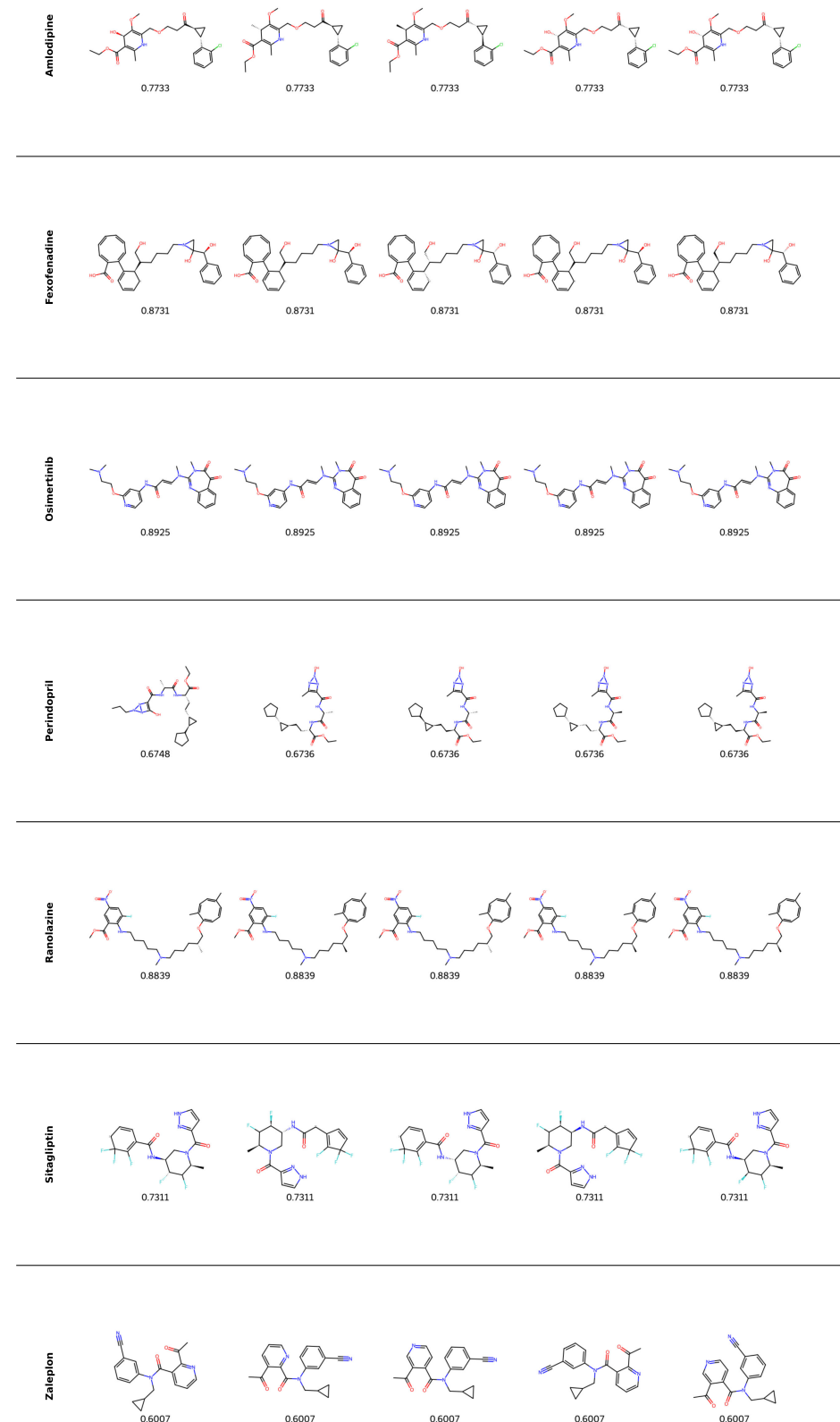


Figure I27: Examples of the generated top-5 molecules from a single run of **NovoMolGen-SMILES-BPE-32M**. The scores are provided at the bottom of each generated molecule.

J. Protein-Ligand Docking

The docking score reflects the strength of interaction between a ligand and its target protein. In this study, we focus on optimizing binding affinity for five human proteins, each implicated in various diseases:

1. **parp1**: Poly(ADP-ribose) polymerase 1 (PARP1) is a nuclear enzyme involved in DNA repair, transcriptional regulation, and cell survival. PARP1 inhibitors are widely studied for cancer therapy, particularly in tumors with defective DNA repair mechanisms.
2. **fa7**: Factor VII (FA7), also known as proconvertin, is a coagulation protein essential for blood clotting. Deficiencies in FA7 are associated with bleeding disorders, including hemophilia-like conditions.
3. **5ht1b**: The 5-hydroxytryptamine receptor 1B (5-HT1B) is a serotonin receptor involved in neurotransmitter regulation. It plays a role in mood disorders, anxiety, and migraine, making it a therapeutic target for psychiatric and neurological conditions.
4. **braf**: B-Raf (serine/threonine-protein kinase B-Raf) is a key regulator of the MAP kinase/ERK signaling pathway, which controls cell proliferation and differentiation. Mutations in BRAF are commonly associated with various cancers, including melanoma and colorectal cancer.
5. **jak2**: Janus kinase 2 (JAK2) is a tyrosine kinase involved in the JAK/STAT signaling pathway, which regulates hematopoiesis and immune function. Mutations in JAK2 are linked to myeloproliferative disorders such as polycythemia vera and essential thrombocythemia.

We employ the docking program QuickVina 2 [Alhossary et al., 2015] to compute docking scores, setting the exhaustiveness parameter to 1. The timeout for 3D conformer generation is set to 20 seconds, while the docking score calculation timeout is set to 50 seconds. Box sizes and center coordinates for the target proteins are taken from Lee et al. [2023]. To compute the maximum Tanimoto similarity with the training molecules, we randomly sample 10 million molecules from the training set and identify the unique and novel compounds. This approach is adopted as searching against the full set of 1.5 billion molecules is computationally infeasible. The novelty results are presented in Table J9 and the visualization of generated novel hits are presented in Figure J29. The reward curve is shown in Figure J28.

Table J9: Novelty comparison on protein-ligand docking tasks. We report Novelty (%), calculated with respect to the ZINC-250k dataset. Results show the mean and standard deviation from 3 independent runs. Baseline data is sourced from Lee et al. [2024b]. **Blue** denotes the best performing model, while **Pink** represents the second-best performing model (p value < 0.05).

Method	parp1	fa7	5ht1b	braf	jak2
REINVENT	9.894 _(2.178)	10.731 _(1.516)	11.605 _(3.688)	8.715 _(2.712)	11.456 _(1.793)
MORLD	98.433 _(1.189)	97.967 _(1.764)	98.787 _(0.743)	96.993 _(2.787)	97.720 _(0.995)
HierVAE	60.453 _(17.165)	24.853 _(15.416)	48.107 _(1.988)	59.747 _(16.403)	85.200 _(14.262)
FREED	74.640 _(2.953)	78.787 _(2.132)	75.027 _(5.194)	73.653 _(4.312)	75.907 _(5.916)
MOOD	84.180 _(2.123)	83.180 _(1.519)	84.613 _(0.822)	87.413 _(0.830)	83.273 _(1.455)
GEAM	88.611 _(3.107)	89.378 _(2.619)	84.222 _(2.968)	90.322 _(3.467)	89.222 _(1.824)
SMILES-32M-ATOMWISE	30.34 _(7.0)	45.84 _(26.0)	15.38 _(2.0)	23.14 _(3.0)	41.48 _(8.0)
SMILES-157M-ATOMWISE	54.31 _(5.0)	46.26 _(8.0)	27.28 _(9.0)	29.01 _(16.0)	44.68 _(4.0)
SMILES-300M-ATOMWISE	37.78 _(16.0)	66.12 _(10.0)	42.69 _(17.0)	33.23 _(18.0)	37.83 _(6.0)
SMILES-32M-BPE	56.28 _(6.0)	62.02 _(6.0)	33.69 _(8.0)	52.73 _(8.0)	48.42 _(7.0)
SMILES-157M-BPE	45.98 _(5.0)	62.06 _(2.0)	43.62 _(4.0)	63.26 _(5.0)	51.64 _(4.0)
SMILES-300M-BPE	50.12 _(9.0)	31.37 _(4.0)	40.44 _(3.0)	53.24 _(3.0)	45.87 _(1.0)

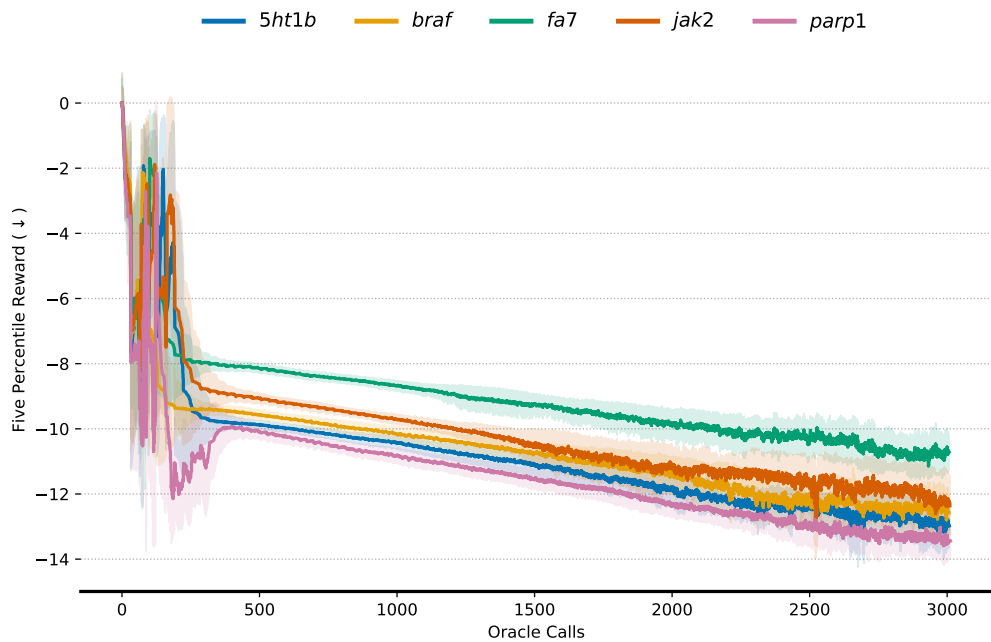


Figure J28: Sample efficiency of **NovoMolGen-SMILES-BPE-32M** on Protein-ligand docking goal-directed generation tasks. The plot tracks the top 5th percentile of the reward distribution as a function of oracle calls, demonstrating our model’s ability to rapidly discover high-reward molecules.

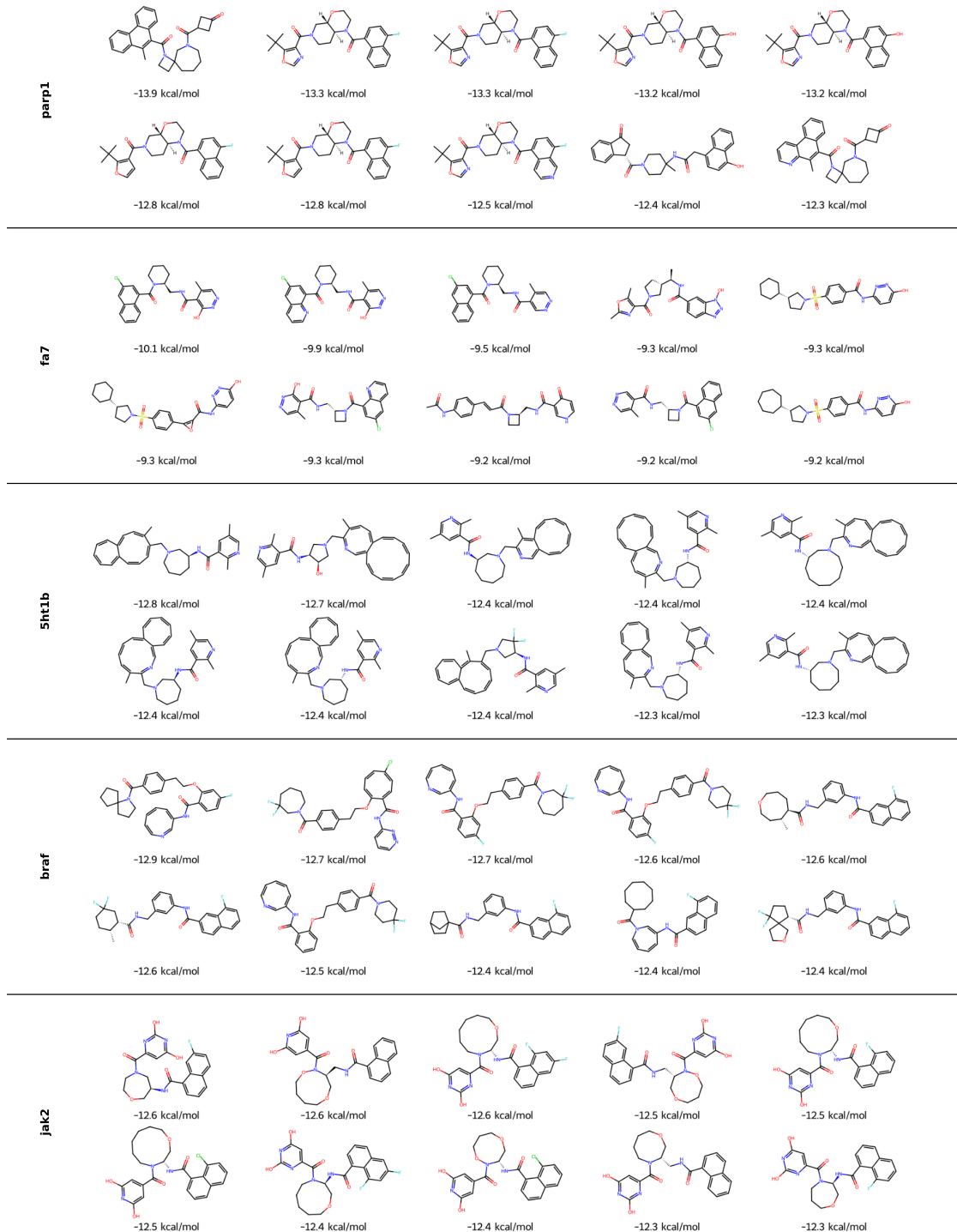


Figure J29: Examples of the generated top-10 molecules ($\text{QED} > 0.5$, $\text{SA} < 4$) from a single run of **NovoMolGen-SMILES-BPE-32M**. The docking scores are provided at the bottom of each generated molecule.

K. BPE Substructures

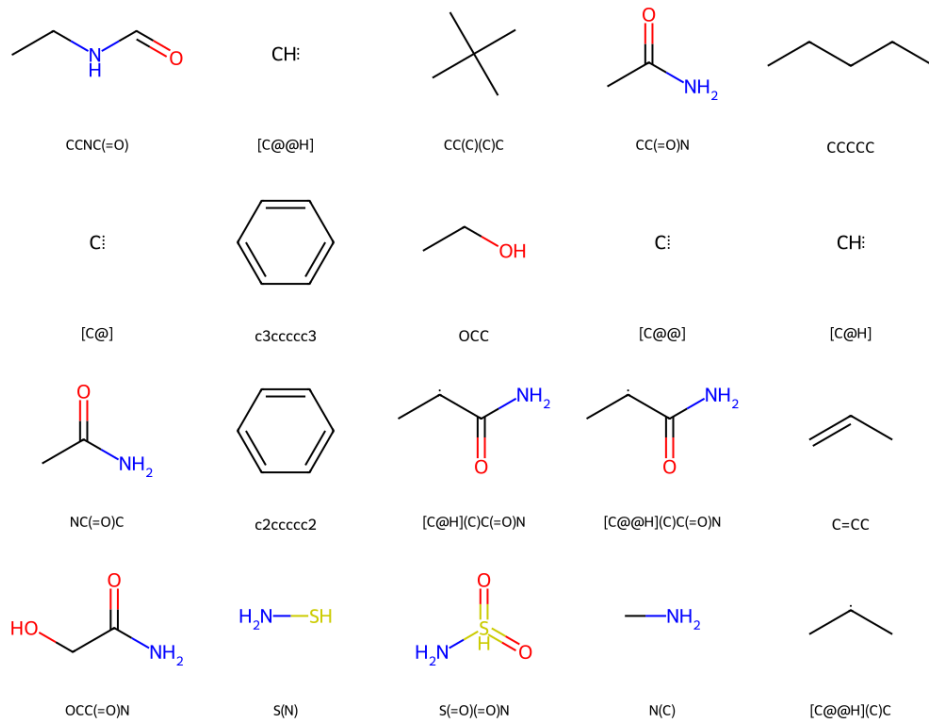


Figure K30: Substructures present in BPE tokenization